BRNO UNIVERSITY OF TECHNOLOGY
VYSOKÉ UČENÍ TECHNICKÉ V BRNĚ

FACULTY OF MECHANICAL ENGINEERING
FAKULTA STROJNÍHO INŽENÝRSTVÍ

INSTITUTE OF PHYSICAL ENGINEERING
ÚSTAV FYZIKÁLNÍHO INŽENÝRSTVÍ

THE ANALYSIS OF LIMITS FOR MULTIMODE FIBRE IMAGING
ANALÝZA LIMITŮ ZOBRAZOVÁNÍ MULTIMODOVÝMI OPTICKÝMI VLÁKNY

MASTER'S THESIS
DIPLOMOVÁ PRÁCE

AUTHOR — **Bc. Hana Štolzová**
AUTOR PRÁCE

SUPERVISOR — **Ing. Zbyněk Dostál, Ph.D.**
VEDOUCÍ PRÁCE

BRNO 2018

BRNO FACULTY UNIVERSITY OF MECHANICAL OF TECHNOLOGY ENGINEERING

Master's Thesis Assignment

Institut:	Institute of Physical Engineering
Student:	**Bc. Hana Štolzová**
Degree programm:	Applied Sciences in Engineering
Branch:	Precise Mechanics and Optics
Supervisor:	**Ing. Zbyněk Dostál, Ph.D.**
Academic year:	2017/18

As provided for by the Act No. 111/98 Coll. on higher education institutions and the BUT Study and Examination Regulations, the director of the Institute hereby assigns the following topic of Master's Thesis:

The analysis of limits for multimode fibre imaging

Brief description:

The diploma thesis is focused on the analysis of limits for multimode optical fibre (MMF) imaging, specifically to explore the influence of the Gaussian beam parameters on imaging within MMFs. As a part of the diploma thesis, the optimal geometry of set-up is designed with respect to the most reliable way of beam parameter control. The computer controlled light shaping and the spatial light modulators (SLMs) are used to compensate for the beam aberrations and control the Gaussian beam parameters.

The goal of the diploma thesis is to confirm the theoretical and simulated limitations for MMF imaging by experiments and provide the reader with substantial information connected with the issue and introduce briefly the experimental methods.

Master's Thesis goals:

1) Find the specific limits for the multimode optical fiber imaging and provide the underlying theory.
2) Carry out a computer simulation of the phenomena.
3) Perform an experiment to confirm the simulation.
4) Analyze the measured data and process the final results of the experiment.

Recommended bibliography:

VELLEKOOP, I. M. and MOSK, A. P., Focusing coherent light through opaque strongly scattering media, Opt. Lett. 32, 2309-2311 (2007).

ČIŽMÁR, T. and DHOLAKIA, K., Shaping the light transmission through a multimode optical fibre: complex transformation analysis and applications in biophotonics, Opt. Express 19, 18871-18884 (2011).

LI, Y., Degeneracy in the Fraunhofer diffraction of truncated Gaussian beams, J. Opt. Soc. Am. A 4, 1237-1242 (1987).

GLOGE, D., Weakly Guiding Fibers, Appl. Opt. 10, 2252-2258 (1971).

Students are required to submit the thesis within the deadlines stated in the schedule of the academic year 2017/18.

In Brno, 24. 10. 2017

VYSOKÉ UČENÍ TECHNICKÉ V BRNĚ FAKULTA STROJNÍHO INŽENÝRSTVÍ DĚKANÁT L. S.

prof. RNDr. Tomáš Šikola, CSc.
Director of the Institute

doc. Ing. Jaroslav Katolický, Ph.D.
FME dean

Abstrakt

Multimódová vlákna jsou zobrazovacím prostředkem s významným potenciálem v in-vivo mikroendoskopii. V poslední době tato metoda zaznamenala velký rozvoj, a to díky zdokonalování výpočetní a jiné techniky, například prostorové modulace světla.

Cílem této práce bylo nalézt specifické limity zobrazování multimódovými vlákny a představit jejich počítačovou simulaci. Byl zkoumán vliv způsobu osvětlení optického systému obsahujícího multimódové vlákno na jeho schopnost fokusace a zobrazování. Analýzou dat získaných ze simulací a experimentu bylo zjištěno, že různá míra omezení Gaussovského svazku a plnění apertury multimódového vlákna má zanásledek významnou změnu zobrazovacích schopností systému. Při pozorování kvality fokusace bylo zjištěno, že nejlépe se projevují svazky málo omezené aperturou vlákna. Tento fakt byl potvrzen i experimentálním měřením. Zobrazování za použití svazků s podobnými hodnotami omezení (50%) projevovalo i nejlepší schopnost přenosu kontrastu. Avšak při analýze rozlišení dvou bodových objektů se jako nejvhodnější projevily svazky významně přeplňující numerickou aperturu vlákna, 100% a více. Přítomnost tohoto rozdílu poukazuje na skutečnost, že multimódové vlákno není zcela náhodné médium, ale propagace světla skrz multimódové vlákno projevuje znaky závislosti na vnějších zobrazovacích podmínkách, jako je například změna omezení osvětlovacího svazku. V této práci bylo představeno několik způsobů vyhodnocení kvality zobrazování pomocí multimódového vlákna. Každé z těchto kritérií podalo dílčí charakteristiku chování optického systému obsahujícího multimódové optické vlákno. Jednotlivé výsledky se neshodují na jednom konkrétním řešení a nutí osobu využívající zobrazovací systém obsahující multimódové vlákno ke zvážení několika aspektů, a to v jakém prostředí bude daný optický systém využívat a který parametr kvality zobrazení bude považovat za nejdůležitější.

Summary

Multimode fibers are the imaging tool of a significant potential in in-vivo microendoscopy. Recently, this method has seen a great development, thanks to the improvements in computational and other technologies, such as digital spatial light modulation. The aim of this work was to find specific limits of multimode fiber imaging and to present their computer simulation. The effect of illumination of the optical system containing the multimode fiber on its focussing and imaging capability was investigated. By analysing the data obtained from simulations and experiments, it has been found that the various levels of the Gaussian beam truncation by a projected multimode fiber numerical aperture results in a significant variance in the imaging capabilities of the system. Therefore, it seems that the multimode optical fibers are not a completely random medium. Observing the quality of the focusing, it was found that low truncated beams (beam-waist around 50% of the projected fiber numerical aperture), have the highest performance. This fact was verified by experimental measurements. Imaging using similarly truncated beams showed the best contrast transmission capability. However, when analysing the resolution of two pointlike objects, the beams with a significantly larger waist and a higher degree of truncation, of 100% or more, were most appropriate. The presence of this difference forces the person using the imaging system containing the multimode fiber to consider several aspects, in what environment the particular optical system will be used and which imaging quality indicator will be considered the most important.

Klíčová slova
mikroendoskopie, zobrazování, přenos kontrastu, rozlišení, multimódové vlákno, optika, fotonika, digitální prostorová modulace světla, náhodná média

Keywords
microendoscopy, imaging, modulation transfer function, resolution, optics, photonics, digital spatial light modulation, random media

ŠTOLZOVÁ, H. *Analýza limitů zobrazování multimodovými optickými vlákny.* Brno: Vysoké učení technické v Brně, Fakulta strojního inženýrství, 2018. 55 s. Vedoucí práce Johanna Trägårdh a Zbyněk Dostál.

I declare that the master thesis submitted hereby is my own work under the supervision of Ing. Zbyněk Dostál, Ph.D. and Dr. Johanna Trägårdh and that all literature sources were quoted completely and correctly.

.....

Bc. Hana Štolzová

I would like to express my sincere gratitude to my first supervisor Ing. Zbyněk Dostál, Ph.D. and external supervisor Dr. Johanna Trägårdh for their support, motivation and advice during writting of my master's thesis. A special gratitude goes to a head of photonics research group in Institute of Scientific Instruments and my Erasmus+ supervisor prof. Tomáš Čižmár. I would like to thank the Complex Photonics Group in Dundee for their advice and support with numerical simulations, planning and realisation of experiment and for very supportive and friendly atmosphere they cerated during my stay in Dundee, Scotland. I acknowledge support from the program and grant Gate2μ CZ.02.1.01/0.0/0.0/15$_0$03/0000476 in Institute of Scientific Instruments (The Czech Academy of Sciences). I was also supported by TU Brno, Institute of Physical Engineering.

Finally, I would like to thank my family and my friends for being in my life and making my life such as interesting and enjoyable as it is.

Bc. Hana Štolzová

Contents

Introduction

Gaining deeper insight into biological tissue lead to essential adaptation of imaging equipment to minimize the tissue demage and preserve the highest possible imaging quality. For a long time many techniques competed in quality and depth in deep tissue imaging and some of them penetrate to a reasonable depth, however, with the loss of the resolution. The optical fibers turned up as a good solution for deep tissue in-vivo imaging, overcoming in penetration depth some other imaging techniques, such as multi-photon microscopy, see fig. 1[1].

An optical fiber is a flexible, transparent glass or plastic fiber. The fiber usually consists of two components, a core with higher refractive index and a cladding with slightly lower refractive index. The signal travels through the fiber by the total internal reflection and it forms light patterns with constant shape but different phase velocities, called modes. The major utilization used to be in the communications, where they permit signal transmission over long distances with low loss. The optical fibers, however, diffused into medicine due to the ability to transport images from hardly-accessible areas, which is highly-valued in biological endoscopy.

For its simplicity bundles of single mode optical fibers were first employed in endoscopy. Later, with the advancement of computational and other technology, such as spatial light modulators etc., the multi-mode optical fibers (MMFs) started to be engaged in deep tissue imaging.

In comparison to fiber bundle, the MMF is significantly less space demanding and the image is less pixelated in contrast to fiber bundle images. In terms of pixelation, however, some of the drawbacks of a fiber bundle can be overcome, e.g. by phase correction [1]. Regardless the immense number of advantages, the MMF imaging method deals with many obstacles which first need to be solved before the technique could be fully utilized in medical science.

One of the most significant steps forward in MMF imaging technology was the digital spatial light modulation expansion. It provided the possibility to pre-shape wave-front of the beam accordingly to the fiber-light-propagation properties, therefore made the MMF imaging feasible. The compensation for MMF modal scrambling and other optical aberrations gives the control over focusing and imaging through MMFs [2]. To maximize the imaging quality, however, all the related conditions need to be optimised.

The aim of this diploma thesis is to tune the illumination conditions, specifically the

[1]The structure of the figure was designed by prof. Mgr. Tomáš Čižmár Ph.D and adapted for purposes of this thesis.

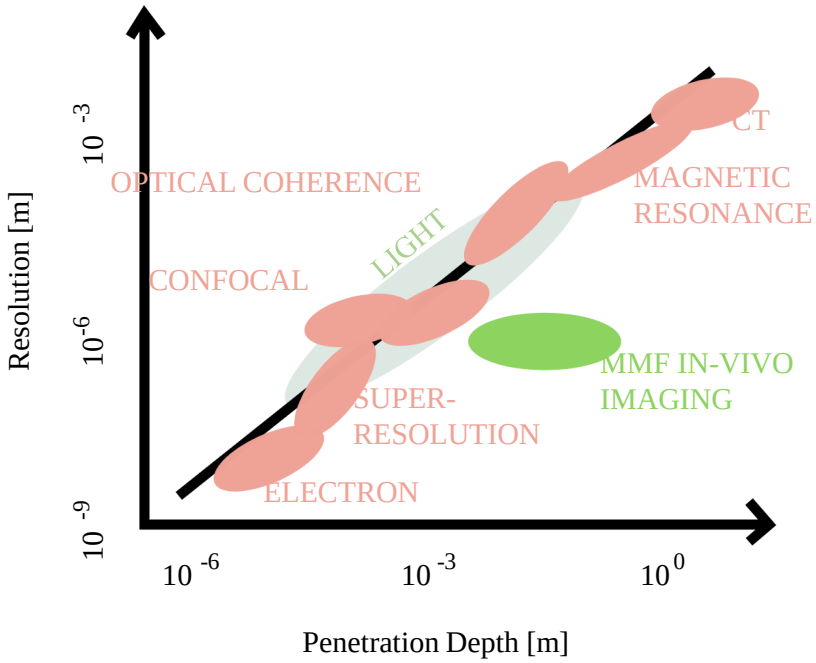

Figure 1: Deep tissue imaging techniques comparison.

degree of overfilling the numerical aperture of the fiber, to reach the highest achievable imaging quality. Moreover, the dependence of imaging properties on the illumination conditions will show that the MMF is not a completely random media.

Three activities are undertaken to identify the most suitable illumination. First, the light propagation within the fiber will be simulated and the optical system enhancement for different beam-shapes will be assessed. Further, the theoretical simulation will be experimentally verified. Finally, the limitations of imaging emerging from different illumination-beam-shapes will be studied. To summarize the goals of the work:

- Find the specific limits for the multimode optical fiber imaging and provide the underlying theory.
- Carry out a computer simulation of the phenomena.
- Perform an experiment to confirm the simulation.
- Analyze the measured data and process the final results of the experiment.

Resulting from the described analyses the dependability of light propagation through MMF on external imaging conditions will be presented. Further work can continue as an experimental study to support research listed here or to apply the knowledge to other MMF imaging experiments.

1. Basic concepts

This diploma thesis aims to comprehensively overview the theoretical background of light propagation within multimode fibers (MMFs) and the use of MMF as an imaging tool. The role of MMF as an imaging medium will bring hereby other issues to explain, such as principles of spatial light modulation, imaging properties and main imaging evaluation criteria.

High demands are placed on the imaging quality, since MMFs intended to be used e.g. as micro-endoscopes for in-vivo applications. To design the highest-quality-MMF imaging system, the most suitable illumination need to be traced. Therefore, the primary problem to be cleared up in this diploma thesis is the illumination requirements optimisation for MMF imaging.

The following theoretical part reviews basic concepts crucial for all the research, such as principles of optical fibers, and optical fiber imaging.

The imaging section will introduce spatial light modulation, the method of focusing and imaging through a fiber. In order to investigate the influence of illumination, in the last part, the properties of the beam will be prefigured and the basic propagation rules of the beam in the MMF optical system will be explained.

1.1 Optical fibers

Optical waveguides and fibers apply the principle of total internal reflection (TIR) to propagate light along material interface. For each waveguide there is an underlay of lower refractive index and a waveguiding layer made of higher refractive-index material ($n_{underlay} < n_{guiding}$), for fulfilling the conditions of TIR. In case of optical fibers the waveguiding component and the underlying material are formed to a thin fiber typically with cylindrical symmetry, where the guiding layer forms a fiber core with the refractive index n_c and the underlying material surrounds the core as a fiber cladding with the refractive index n_{clad}, where $n_{clad} < n_c$. The TIR appears when the light is coming from optically denser medium to optically sparse material and it is fully reflected back to the material with higher refractive index. In fiber optics the light entering the fiber is fully reflected from the core-cladding interface and therefore travels through the fiber. An incident angle of light striking the interface is larger than the critical angle, α_{crit}. The refractive indeces determine the sine of critical angle α_{crit} and numerical aperture NA of the fiber:

$$\alpha_{crit} = \arcsin \frac{n_{clad}}{n_c}, \tag{1.1}$$

$$NA = \sqrt{n_c^2 - n_{cald}^2} = \alpha_{crit}. \tag{1.2}$$

Depending on the refractive indeces profiles there exist three main kinds of fibers: multimode step index, graded index or singlemode step index fiber, see fig. 1.1. The refractive index in step-index fibers is changing abruptly from core to cladding while the graded-index fiber uses smoothly changing refractive index to equalize the mode phase velocities. The smooth refractive index transmission force the rays to travel from end-to-end simultaneously causing different pathways, as it is shown in fig. 1.1. The MMFs are often considered as a randomly scattering media (random media) that propagate the light by many paths of random phases and directions [3]. However, in this diploma thesis we show that the light propagation in MMF is not entirely random.

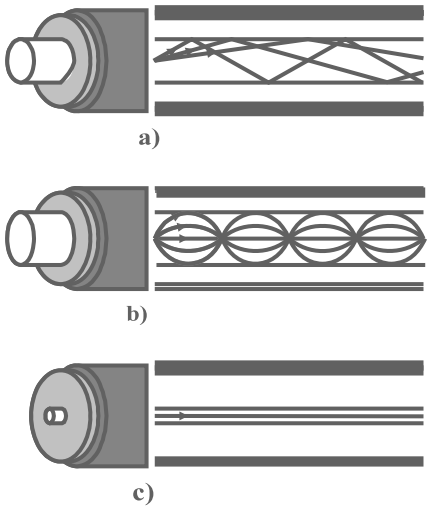

Figure 1.1: Optical fiber types. Sub-figures (a), (b) and (c) represent multimode step index fiber, multimode graded index fiber and simgle mode step index fiber, respectively.

1.1.1 Fiber modes

When the light enters a multimode step index optical fiber, it splits into limited number of propagation invariant modes (PIMs) which travel with different phase velocities. PIMs are specific patterns of electric field preserving a constant shape while travelling through the fiber. Each of the modes is consistent in shape but travels with a different phase velocity, this causes a loss of a phase relationship between parts of the initial image entering the fiber. Therefore, the final image on the output of the fiber is an

interference pattern made of delayed modes, called a speckled pattern. However, there is a deterministic connection between the light pattern on the input and output of the fiber which could be analysed and later used to decode the speckled pattern to the original image again. This procedure produces the so-called transmission matrix T.

Optical fibers used for imaging commonly have a small difference between refractive indeces of core and cladding (in order of hundredths). Therefore, they are considered as weakly guiding fibers and their modes are usually described as linearly polarized (LP) modes. In case of strongly guiding fibers the transverse electric and transverse magnetic modes would need to be distinguished[1].

The use of LP modes then simplify a mathematical description of the fields' shapes using a characteristic equation [5] for the core and cladding modes:

$$\left(\frac{u}{n_c}\right)\left(\frac{J_{l\pm1}(u)}{J_l(u)}\right) = \pm\left(\frac{w}{n_{clad}}\right)\left(\frac{K_{l\pm1}(w)}{K_l(w)}\right), \tag{1.3}$$

where $J_l(u)$ and $K_l(w)$ are Bessel functions of order l and they describe the field distribution inside the core and the cladding respectively. Parameters u and w contain propagation constants β and refractive indeces for core and cladding modes, respectively and stand for following equations:

$$u = a(k^2 n_c^2 - \beta^2)^{\frac{1}{2}}, \tag{1.4}$$

$$w = a(\beta^2 - k^2 n_{clad}^2)^{\frac{1}{2}}, \tag{1.5}$$

where the k is a wave number and a is a fiber aperture radius.

Assuming the continuity of core and cladding modes on the interface the solution for equation 1.3 provide the propagation constants β for each fiber mode [5]. In ideal situation, such as when the fiber is free of any defects, the knowledge of propagation constants and the length of the fiber gives enough information about light propagation within the fiber and the transmission matrix could be calculated. If there exist some fiber imperfection the simulation is broaden of corresponding parameters.

1.1.2 Transmission matrix

The first theoretical and experimental approaches for wavefront modulation were based on iterative algorithms or phase conjugation, however, the introduction of a transmission matrix T meant a simplification of the calibration process for use of MMF [6].

The matrix T describes a linear relation between input pattern E^{in} and output pattern E^{out} of MMF, see fig. 1.2. Therefore, it gives a complete information about light propagation through the MMF. The T can be defined for a given wavelength as a matrix of complex coefficients t_{mn} connecting the phase and amplitude at the nth input element to mth output element [7]. The output pattern E^{out} is given by:

[1] Only either the electric or the magnetic field is perpendicular to the optical axis [4].

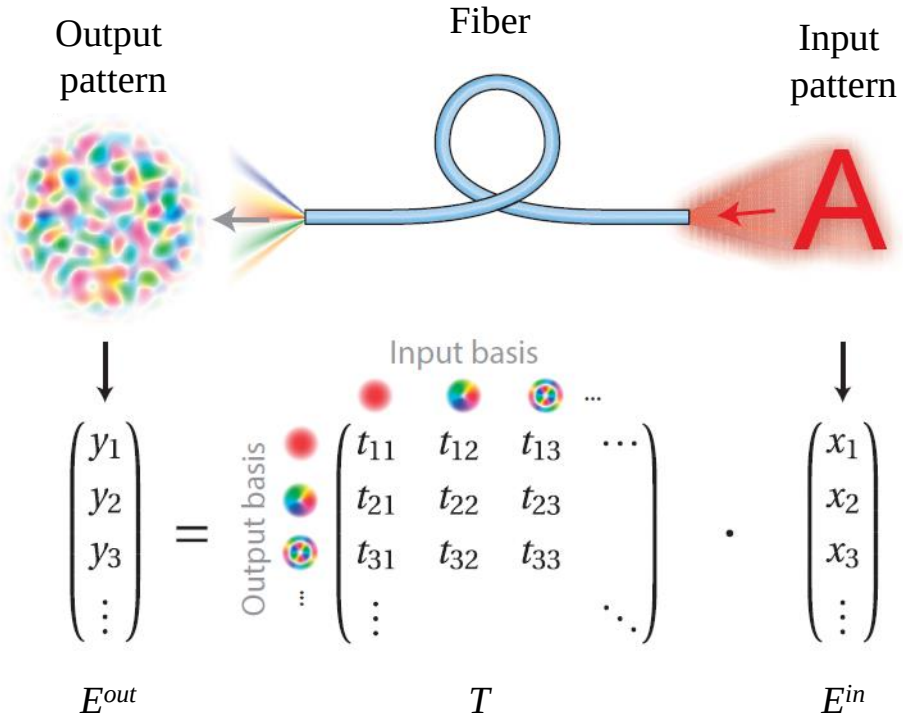

Figure 1.2: Transmission matrix T. The picture is outsourced from [8]. The E^{in} is an object to be propagated and E^{out} is a resulting output pattern of the propagation.

$$E_m^{out} = \sum_n^N t_{mn} E_n^{in} \tag{1.6}$$

where the E^{in} is the complex amplitude of the optical field in the nth modulated input mode [9, 7]. The T matrix consists of ordered input and output basis and creates an orthogonal system.

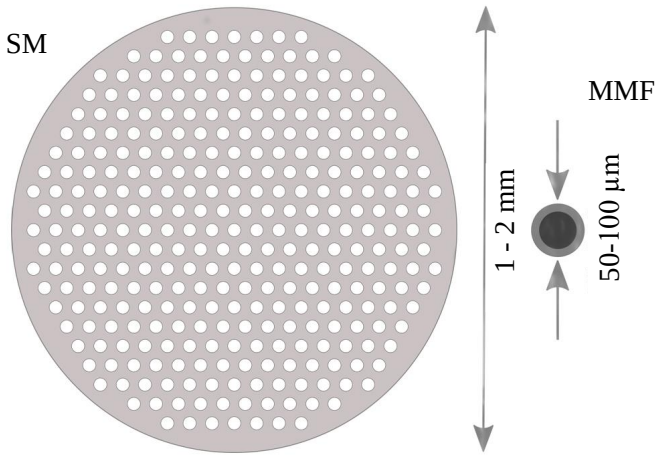

Figure 1.3: Imaging equipment diameter comparison. Comparison of the singlemode fiber budle SM and the multimode fiber MMF diameters.

1.2 Principles of optical fiber imaging

The bundle of singlemode fibers came to mind as an imaging tool long time ago. Each singlemode fiber gives a pixel of an imaged object and the images could be directly interpreted. However, the invasiveness of the bundle was excessive for it to serve for deep tissue imaging. For these purposes, the development of micro-endoscopy focused more on the evolution of MMF imaging method. The comparison of the diameter of the fiber bundle and MMF can be seen in fig. 1.3[1].

The first attempt of MMF imaging was based on reconstruction of the fiber properties and sending the phase conjugated signal of this fiber away from the place of interest [10]. The method uses two supposedly same pieces of MMF one for imaging and one for creation of the phase conjugated signal. However, it is sensitive to any coupling between propagation modes of MMFs and it needs a very precisely manufactured fibers. Further idea was to separate each mode of the fiber and accordingly to its phase delay pre-shape the input light [11]. This method, however, does not deal with the mode mixing. An idea of holographic projection within MMF came to mind. The holograms of points are projected on the sample and the reconstructed picture could be observed. The recent imaging method utilizes the computer-processed calibration of holographically analysed points and then scans with these points across the sample.

It is possible to use these approaches to gain deep tissue images with MMFs [12] with the development of the digital spatial light modulation.

The next part, therefore, will be oriented to explanation of the principles of focusing and imaging through MMF and further the fundamental aspects of digital spatial light modulation.

[1] Author of the figure: Dr. Sergey Turtaev.

1.2.1 Focusing through multiomode optical fiber and image transmission

Since the MMF imaging systems are the scanning imaging tools, it is required to scan with the light over the output facet of the fiber. In order to do so the light is forced to interfere constructively at a focal spot, also called output mode. For each output mode with different position a suitable phase-grating need to be applied to the spatial light modulator (SLM).

To find an appropriate diffraction mask (DM) for each focal point, the pattern on SLM undergoes a testing procedure when different DMs are applied. There exist two main procedures to manipulate with the wavefront, the sub-domain method (used for the experiment in this diploma thesis) and the method of truncated plane-waves. The principle of testing is the same for both techniques with only a few differences. For the sub-domain technique the area of SLM is divided into finite number of sub-domains and each sub-domain form one input mode. By contrast, the plane-wave method uses the entire area of SLM for creation of one input mode.

By the analysis of interference pattern (the resulting pattern created by input modes and the reference beam) recorded on CCD chip, the appropriate DM is traced. The interferometric measurements of each tested input mode are performed with phase-steps of $\pi/2$, for two periods, 4π [6]. The DM giving the highest intensity at the chosen CCD pixel is established as the most convenient and stored for further use [2]. The process is repeated for all input modes and recorded DMs are later applied to scan the focal spot across the output of the MMF. In simulation, the focal points are created by backward transmission (explained in detail in part 3.1).

When the focal points on distal facet of the fiber are created the image transmission could be performed. The image is scanned with the previously calibrated focal spots. The known position of the focal point and intensity of the imaged target at that point give all information needed for the image reconstruction.

The focal points are created using phase-only or phase and amplitude modulation with employment of the digital spatial light modulation. Therefore, the following part will introduce basic principles of digital spatial light modulation.

1.2.2 Digital spatial light modulation

Digital spatial light modulators are transmissive or reflective pixelated devices that enable creation of two dimensional patterns (diffraction masks) and by the principle of diffraction allow modulation of light properties (amplitude, phase or polarization). Generally, SLMs have multiple utilizations such as an encoding component for holographic data storage, a wavefront modulation device for holographic optical instruments and holographic tweezers [13]. In terms of MMF imaging, the spatial light modulation is employed to measure and apply the matrix T and to scan the focal spot across the distal fiber facet.

Spatial light modulators

There are many different types of SLMs, such as liquid crystal spatial light modulator (LC-SLM), digital micro-mirror device (DMD) or ferroelectric modulator. For an overview, the two fundamental types of SLMs (LC-SLM and DMD) are introduced.

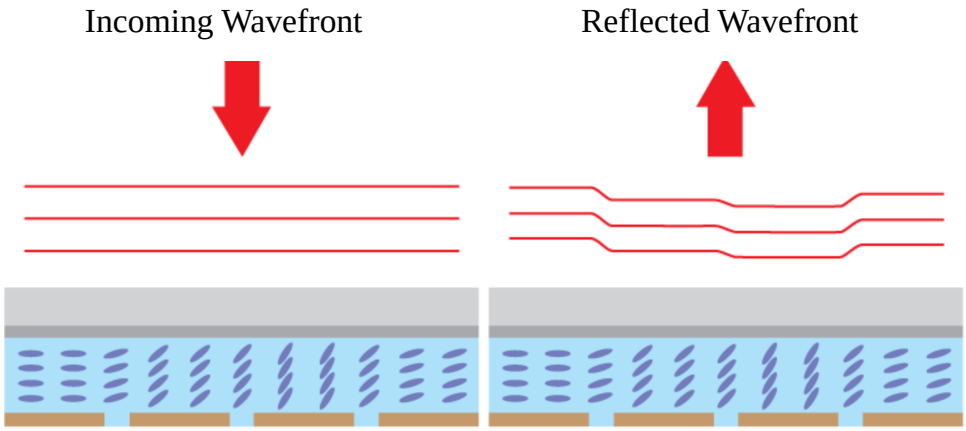

Figure 1.4: Phase modulation with LC-SLM [14].

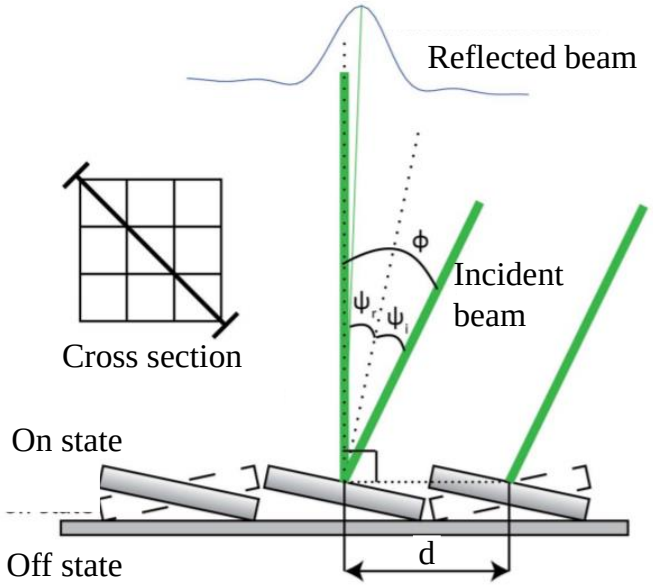

Figure 1.5: Spatial light modulation using DMD [15].

LC-SLM is due to its depth of 8-12 bits a suitable choice for a phase modulation. The phase mask could be applied and the phase is changed smoothly. The phase of incident wavefront is delayed due to different position of liquid crystals, see fig. 1.4, and each section of the wavefront gain a corresponding phase delay.

DMD, on the other hand, is a binary modulator and has mostly been used only for amplitude modulation, see fig. 1.5. Now, however, it can also be used to replace the phase modulation, by applying a binary mask to eliminate the destructively interfering

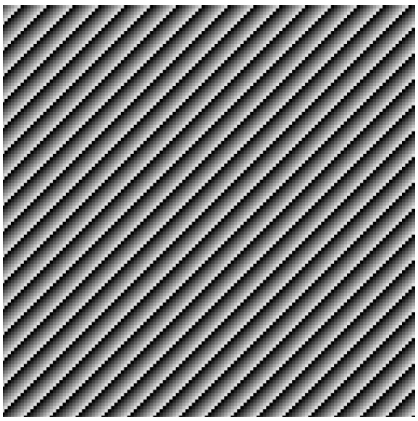

(a) Plane phase mask.

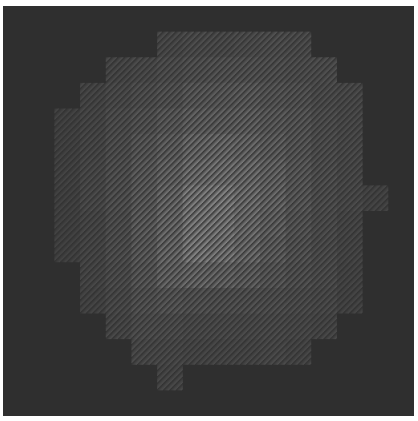

(b) Sub-domains diffraction mask.

Figure 1.6: Diffraction masks.

light from the observed area. The power efficiency of such modulation is significantly lower than the phase modulation. The advantage of DMD, however, is the rate of refreshment. Compared to LC-SLM, DMD is a significantly faster modulator [6].

In this work the emphasis is on the accuracy of modulation, not speed, therefore the LC-SLMs are employed. The phase is modulated using the above-described digitally generated DMs.

Principles of spatial light modulation in complex photonics

A optical principle of diffraction is vital for spatial light modulation. A DM is an optical component with a periodic structure that diffracts light into several diffraction orders travelling in different directions. The DM could be used either to separate colours of white light or to diffract laser light.

One of the first computer-generated DMs were published earlier by Lee [16], therefore it is often called Lee holograms. The pattern of Lee hologram periodically varies between values from $-\pi$ to π, as it is shown in fig. 1.6a, where $-\pi$ corresponds to black colour and π to white colour [17].

In order to combine both information, the phase and amplitude, several methods can be used. The first is an iterative method, the Gershberg-Saxton algorithm. Another possibility is that the mask may vary not only in periodicity and angle but also in intensity, the reflected light then changes in amplitude at the same time as in phase [18]. For the purposes of this work, this principle is used for pre-modulation of the Gaussian beam, therefore the modulation is considered as phase and amplitude modulation.

To achieve phase or amplitude modulation, the DM of specific parameters are applied. The properties of DM are derived from the holographic calibration. Both, the modulation and the calibration, either can be preformed by plane-waves or with the use of sub-domains, shown in fig. 1.6b[2].

The calibration of MMF optical systems is using principles of off-axis holography.

[2]The plane-waves are utilizing all pixels of SLM at ones to create an input mode. For the sub-domain technique the area of SLM is divided into sub-domains separately forming the input modes [2].

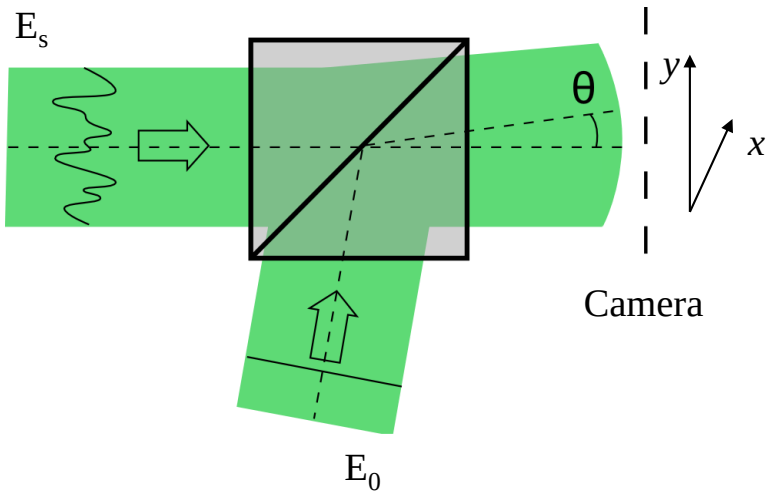

Figure 1.7: Off-axis holography [19].

In off-axis holography the two beams, signal and reference beam, see fig. 1.7, form a small angle and create a hologram. The hologram, as an intensity pattern $I(x,y)$ is recorded on a CCD chip and is given by:

$$I(x,y) = \underbrace{|E_0(x,y)|^2 + |E_s(x,y)|^2}_{order\ 0} + \underbrace{E_0(x,y)E_s^*(x,y)e^{ik\sin\theta x}}_{order\ +1} + \underbrace{E_0(x,y)^* E_s(x,y)e^{-ik\sin\theta x}}_{order\ -1}, \tag{1.7}$$

where $E_0(x,y)$ is a plane-wave, $E_s(x,y)$ is a signal wave and θ is the off-axis angle [19].

Power efficiency of optical systems containing random media using phase modulation

In order to measure the performance of system the ratio between the power in focal spot compared to the overall output power was used as a metric. The power ratio (PR) enables to estimate the percentage of power contributing to a signal and the one forming the background in the intended application [6].

The light propagating in a complex random media could be described as a number of allowed propagating modes. In fibers the modes are propagation invariant modes (PIMs), which means that the modes conserve its properties when propagating through MMF. All the PIMs would need to be controlled by SLM to utilize all the available optical power propagated through MMF. The MMFs have a comparable number of PIMs as the number of SLMs pixels is, thus the modulation is reasonably successful. If the fiber is considered to be a randomly propagating medium, the PRs are approaching the normal Gaussian distribution. Assuming that nearly all the independent input modes of such a systems are controlled with the phase modulation, it has been shown that the power efficiency drops to the value of $\pi/4$ (≈ 0.78)[3] [20, 9]. The phenomena is introduced in following equations.

[3] A detailed explanation of the theoretical limitations of phase modulation can be found in article [9]. Hereby only the fundamental relations will be shown.

The intensity sum of output field s^{out} of a system focusing the input lth component on the jth output pixel can be defined as described in equation 1.8. Based on principles of phase conjugation, where the resulting field has a reversed propagation but conserves the phase and amplitude information, following equations could be expressed:

$$|s_m^{out}|^2 = \left| \sum_l^N k_{ml} k_{jl}^* \right|^2 , \tag{1.8}$$

where $k_{ml,jl}$ is a complex coefficient of matrix K, m and j are indexes of the input or output modes, respectively. N is the number of channels of the observed system [7]. For $m \neq j$, the average intensity $\langle |s_{m\neq j}^{out}|^2 \rangle$ can be described as:

$$\begin{aligned} \langle |s_{m\neq j}^{out}|^2 \rangle &= \left\langle \sum_{l,l'}^{N,N} k_{ml} k_{ml'}^* k_{jl}^* k_{jl'} \right\rangle \\ &= \left\langle \sum_l^N |k_{ml}|^2 |k_{jl}|^2 \right\rangle + \left\langle \sum_{l\neq l'}^{N,N} k_{ml} k_{ml'}^* k_{jl}^* k_{jl'} \right\rangle \\ &= N(N-1)\langle |k|^2 \rangle^2 + N\langle |k|^4 \rangle \\ &\approx N_2 \langle |k|^2 \rangle^2 \qquad\qquad \forall N \gg 1. \end{aligned} \tag{1.9}$$

For $m = j$, the averaged intensity $\langle |s_{m\neq j}^{out}|^2 \rangle$ is calculated as follows:

$$\begin{aligned} \langle |s_{m\neq j}^{out}|^2 \rangle &= \left\langle \left(\sum_l^N |k_{jl}|^2 \right)^2 \right\rangle \\ &= \left\langle \sum_l^N |k_{jl}|^4 | \right\rangle + \left\langle \sum_{l\neq l'}^{N,N} |k_{jl}|^2 |k_{jl'}|^2 \right\rangle \\ &= N(N-1)\langle |k|^2 \rangle^2 + N\langle |k|^4 \rangle \\ &\approx N_2 \langle |k|^2 \rangle^2 \qquad\qquad \forall N \gg 1. \end{aligned} \tag{1.10}$$

Calculation of the output averaged intensities for $m = j$ and $m \neq j$ is:

$$\langle |s_{m\neq j}^{out}|^2 \rangle = N\langle |k|^2 \rangle, \tag{1.11}$$

$$\langle |s_{m=j}^{out}|^2 \rangle \approx N^2 \langle |k| \rangle^2 \qquad \forall N \gg 1, \tag{1.12}$$

and their ratio together with the number of modulated modes give the signal to noise ratio of the resulting intensities.

For calculation of the power ratio PR:

$$PR = \frac{P_f}{P_{out}}, \tag{1.13}$$

where P_f is a power in a focal spot and P_{out} is a total output power a special case is

obtained. When N is approaching very high values, the distribution tends to the limits of Gaussian distribution of $\langle|k|\rangle^2/\langle|k|^2\rangle = \pi/4$ [21], i.e. $PR \approx 0.78$.

As an illustrative example the transmission matrix T of 100 random orthogonal modes was created and used for phase-only modulation. In fig. 1.8 it can be seen that the mean value of relative intensity is approaching 78.7% which is in a good agreement with the theoretical limit of approximately 78.5%.

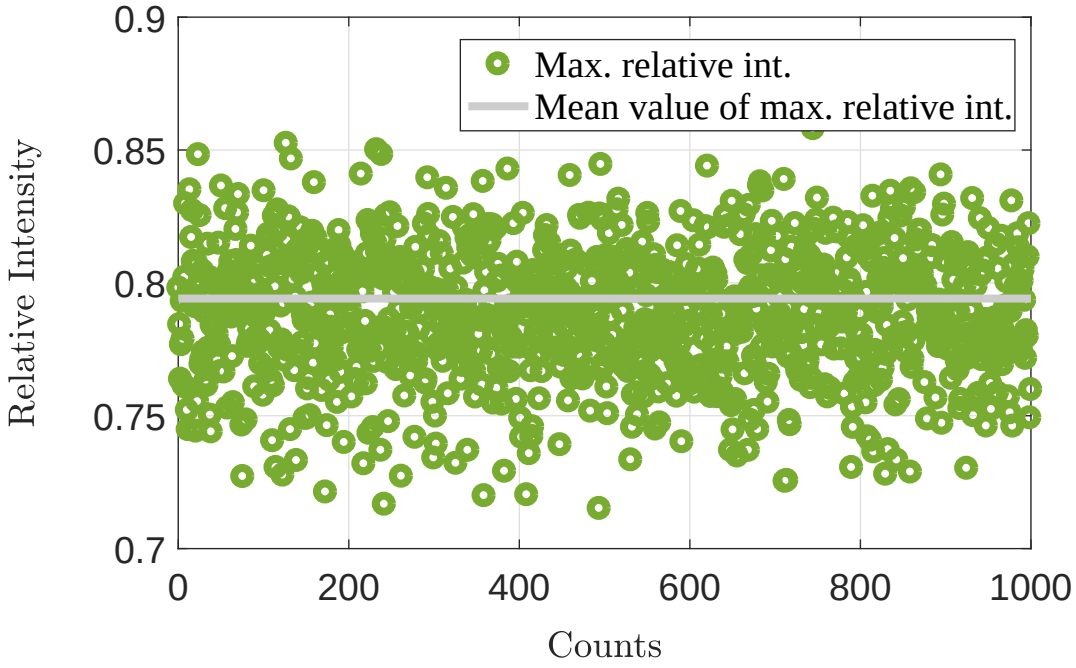

Figure 1.8: Maximal relative intensity for 100 random modes.

However, in this diploma thesis, we show that the PR values perform significant deviations from the normal Gaussian propagation when changing the illumination conditions. This is probably due to the fact that the MMF is not only a random medium, but it does show signs of a predictable light propagating.

Enhancement of optical systems using the liquid crystal spatial light modulators

The maximum reachable enhancement provided LC-SLM is further affected by the random dispersion on liquid crystals, the non-linearity of the diffraction efficiency and other aspects. A detailed description of a diffraction capability can be found in [22, 23].

The performance of LC-SLM drops compared to the perfect phase-modulation systems. In this diploma thesis Meadowlark (HSPDM512) LC-SLMs were used. In experimental part (3.2) it is shown that the values of enhancement, the PR, do not reach the theoretically predicted values but remain approximately 13% lower.

1.2.3 Imaging evaluation criteria

To asses the performance of the MMF imaging system the parameter of PR is employed. However, for the imaging quality evaluation there exist other officially respected criteria.

The most known and used is a criterion of resolution. It attests to the capability to distinguish between two separate objects and tells how close could the two object be to be clearly resolved by optical system. Another very important indicator of imaging quality is a contrast transmission. The dependence of contrast modulation on spatial frequencies imaged with the system is expressed by a modulation transfer function (MTF).

In case of MMFs, the image is also affected by the appearance of unwanted circularly-symmetrical intensity fluctuations of unclear origin. Therefore, there arises the need for the analysis of their influence on imaging.

Further in this part, all the mentioned criteria will be briefly introduced. Later in the thesis, they will be separately used as parameters for assessment and establishment of the most suitable illumination for MMF imaging.

Resolution

There are many factors influencing resolution of the system like NA, refractive indeces or the way of definition of the resolution criteria. The most common is a Rayleigh resolution criterion. The Rayleigh criterion for the minimum resolvable detail is expressed in equation:

$$\sigma_R = 1.22\frac{\lambda}{D}, \tag{1.14}$$

where σ_R is a lateral resolution of the two objects to be resolved, D is diameter of lens and λ is a wavelength of incoming light. Two objects are considered resolved if the minimum in the resulting image does not exceed 80% of the neighbouring maxims.

In case of MMF the resolution criteria is given by the k_{max} which is the maximum spatial frequencies (SFs) in Fourier domain feasible to transmit with the fiber core with numerical aperture NA and wavelength λ [24]:

$$k_{max} = 2\pi\lambda NA. \tag{1.15}$$

For our purposes, when the resolution of the resulting image is evaluated, it is convenient to apply common optical system resolution criteria and the Rayleigh criterion is considered. The intensity difference is referred as a parameter of modulation depth δ. It specifies the two-point distinguish ability, where higher modulation values mean better resolution:

$$\delta = \frac{p_{min}}{p_{max}}100\%, \tag{1.16}$$

where p_{min} is the lowest peak intensity prominence and p_{max} is the highest intensity prominence.

Contrast and modulation transfer function

The quality of imaging could be characterized by the ability to transfer contrast from the specimen SFs to the image plane. This characteristics is called modulation transfer function (MTF). MTF is often used as a description of the imaging system for its compactness, the contrast and resolution are both measured at the same time.

The MTF is possible to use for characterizing any photonic system including MMFs. The standard way of computing the MTF is to estimate contrast C of the imaged structure consisted of different SFs.

$$C = \frac{I_{max} - I_{min}}{I_{max} + I_{min}}, \tag{1.17}$$

where I_{max} and I_{min} are the maximal and minimal intensity values in the image, respectively.

The number of spacings per unit interval (here the cycles of black and white stripes per core diameter, see tab. 4.1) in a specimen is referred to as the SF [25]. In biological microscopy the structure of the specimen need to be resolved and the high SFs is required to transmit the image with the highest contrast possible.

A perfect optical system would have a MTF of unity at all SFs. According to optical aberration and other imperfections the MTF always drops for high SFs and gain a zero value for a very high SF.

As it will be shown in further part 4.4 of this diploma thesis, the MTF for the MMF could be significantly improved by changing the truncation conditions of MMF optical system illumination.

1.3 Beam properties

To complete a brief overview of the theoretical information that is needed for orientation in this research, the illuminating beam properties will be mentioned.

In my diploma thesis the most common type of the beam, the Gaussian beam, is employed and manipulated to change the illumination conditions for the simulations and experiment.

1.3.1 Gaussian beam

Most lasers propagate with the shape of a Gaussian beam. It is a fundamental mode of optical resonators. The relative electric field distribution $E_s(r,z)$ for beam amplitude $|E_0(r,z)|$ at distance $z = 0$ is given by:

$$E_s(r,z) = E_0(r,z)\exp\left(-\frac{r_z^2}{w_0^2}\right), \tag{1.18}$$

where r represents the perpendicular distance from the axis of propagation [26] and w_0 is a beam-waist, the distance from optical axis at which the beam intensity drops to $1/e^2$ relative to its on-axis value [26, 27].

A propagation of the beam is modulated by the optical components. The wavefront is altering with the shape of the transmitted optical surface, the diameter of the aperture, see fig. 1.9 or the numerical aperture of the optical components. In case of MMF optical system, the beam could be limited e.g. by a NA of the fiber, see fig. 1.10. In this diploma thesis the relation of beam-waist to the projected NA of the fiber is expressed by the factor of overfilling OF. The calculation of OF is performed at the SLM plane. A projected beam-waist size w_{bp} and the projected NA of the fiber P_{NA} are considered as the input parameters:

$$OF = \frac{w_{bp}}{P_{NA}}100\%. \tag{1.19}$$

The higher OF the more plane-wave-like and truncated the beam is. In fig. 1.11, there are shown the Gaussian beam profiles used for all the further simulations.

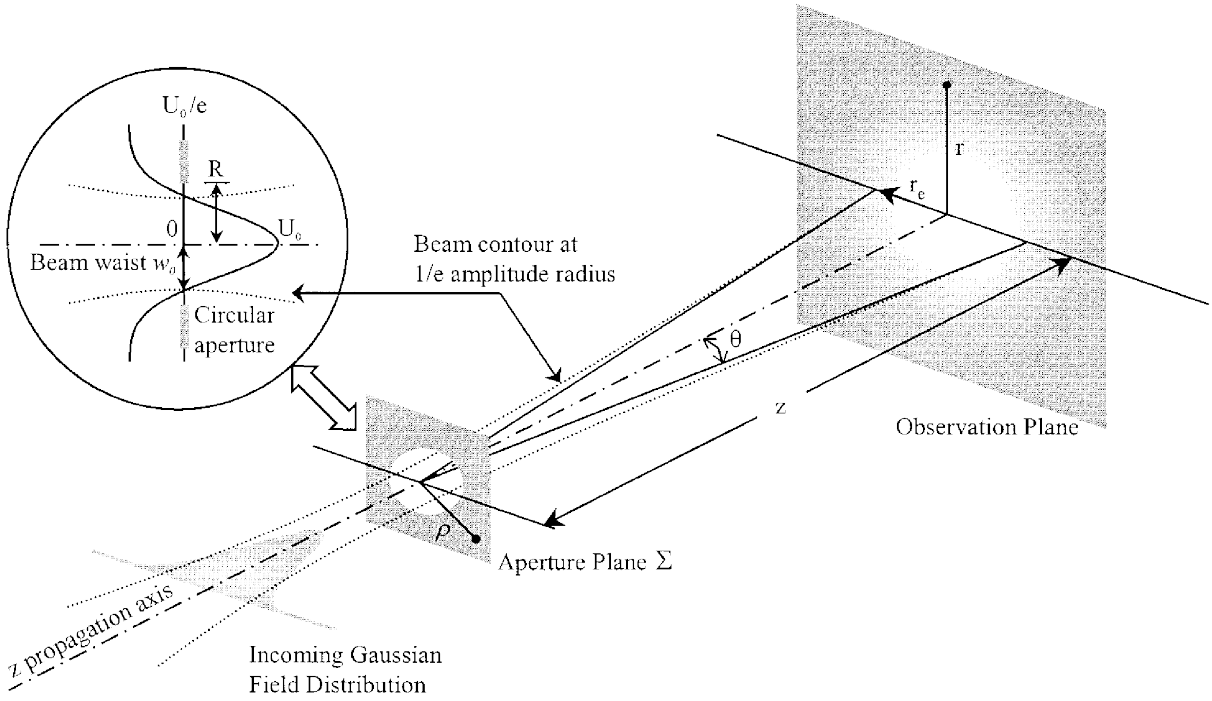

Figure 1.9: Gaussian beam truncation by the aperture of the optical system. The figure is taken from [28]. In the left top corner detail, the w_0 is a beam-waist and R ai a diameter of the truncating aperture, U_0 is the amplitude.

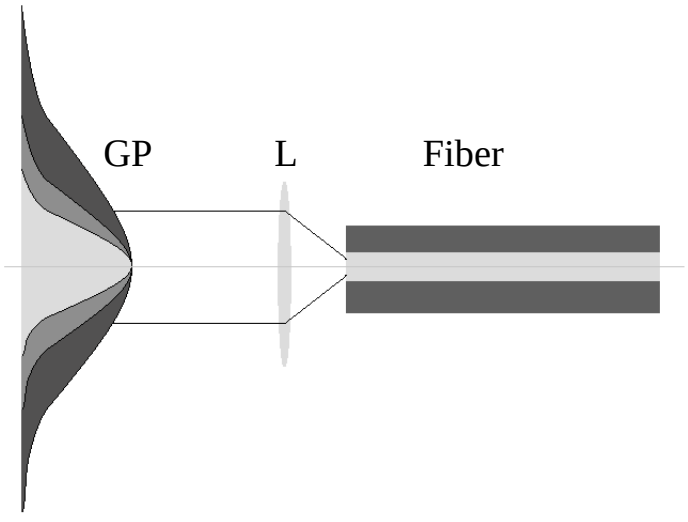

Figure 1.10: Overfilling of the projected fiber aperture. GP are different Gaussian profiles applied on the SLM, L is a lens and Fiber is a MMF. The truncation of the beam by the projected fiber *NA* is shown.

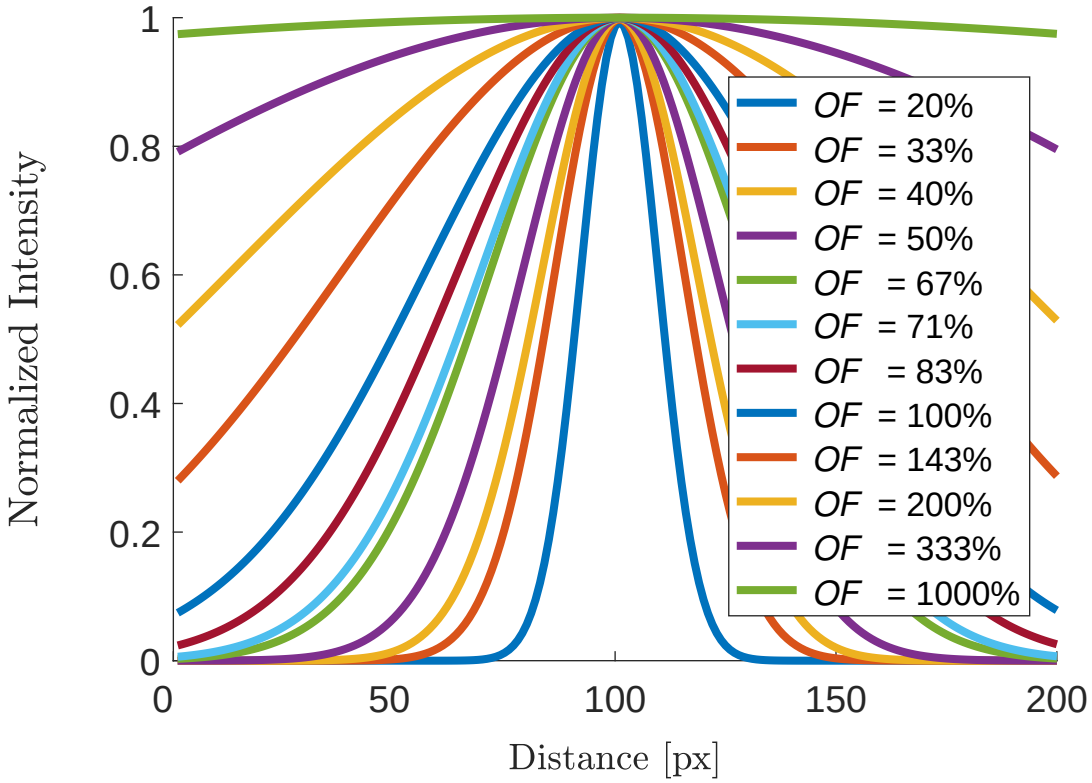

Figure 1.11: The Gaussian profiles used for simulations. The beam-shapes are described directly as OFs, projected beam-waist to projected fiber NA. The radius of projected fiber NA is constant and the beam-waist is changing. For purposes of diploma thesis the fiber $NA = 0.22$ is approximately of a radius 50 pixels in the SLM plane.

2. Properties of optical simulations

After completing the overview of the basic theoretical concepts the experimental tools will be introduced. The subsequent part is built to discuss the methods of numerical optical simulations.

The simulations are divided into two main parts, where each of them perform a methodical step for MMF imaging.

The first simulation, which will be presented in section 3 (Focusing through multimode optical fiber), represents the projection of focused spots and shows the influence of the beam truncation on power ratio (1.2.2) of the foci. This simulation is verified by an experiment.

The subsequent and the main part of the simulations, introduced in section 4 (Limitations of multimode fiber imaging), deals with the use of MMF as an imaging tool. The limitations of MMF imaging depending on the SLM illumination and beam truncation will be demonstrated and interpreted. As a result of the second simulation the most suitable beam for illumination will be determined for each evaluation criteria.

The techniques for optical waves propagation analysis could be performed with analytic solutions or numerical simulations.

At the first stage of this work, unsuccessful attempts to create a precise analytical solution were undertaken. The process lead to the use of approximations of the Lommel and Sturve functions [29] and the conclusion did not provide any precise solution. The application of analytic methods on the problem of beam truncation moreover brought inaccuracy and prolongation of the computational time without any significant positive impact on the analysis. That is why for this diploma thesis the simulations were chosen as an appropriate research method.

Nevertheless, the simulations in optical diffraction are using discrete Fourier transforms, thus the samples with a finite-sized grid. The choice of sampling significantly influences the result of the simulation. In this work sampling is always chosen with respect to the reliability of the simulation results. Therefore, the compromise between the speed and accuracy of computing needs to be made [30]. Selected was the lowest sampling for which the results did not change.

3. Focusing through multimode optical fiber

In order to determine the best conditions for imaging, the performance of the optical system must first be investigated. This section examines the focusing ability of the system and focal points properties. At the end of this section, we will know whether there is any dependence of MMF focusing ability on the overfilling factor and what are the limits resulting from usage of different OFs.

3.1 Simulation

The first simulation is aimed to obtain the focusing ability characteristics of a MMF optical system. Assuming that the MMF imaging is a scanning imaging technique it is needed to create a set of foci which are then scanned over the image.

The virtual set-up (VS), shown in fig. 3.1, was simulated in MATLAB and the light was propagated through it[1]. To characterize the light transmission through the VS, a backward propagation of an ideal point has been applied.

The idea of the backward propagation builds on a fact that the observed object does not deteriorate while being imaged by a perfect optical system. A desired result of a propagation through any optical system is a perfect projection of observed objects on the output of the system. However, due to the optical aberrations, light interactions and other aspects the resulting image is specifically affected. Either the phase or amplitude could be modified.

The degree of image deterioration gives an information about the optical system and its behaviour. In other words, a predefined object is propagated from output to input to obtain the simulated optical system characteristics. This method is commonly used for optical system analysis and it was applied for the purpose of both simulations discussed hereby.

3.1.1 Methods

The transmission matrix (T at the fig. 3.1) is a description of the examined piece of fiber, the 2D fast Fourier transform (FFT) is a representation of a lens which is transforming the propagated image to the Fourier plane, the SLM plane. Due to this

[1] The MATLAB code of the VS with comments can be found in attachments.

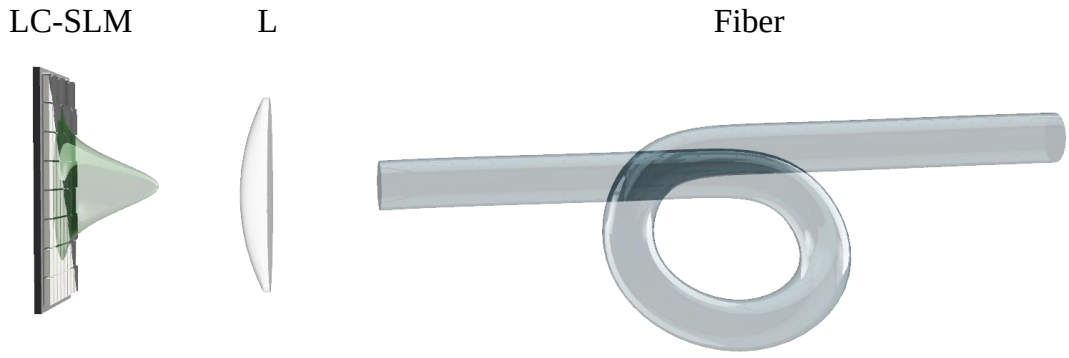

Figure 3.1: Virtual set-up. The fiber represents transmission matrix T, L: lens stands for FFT (a 2D fast Fourier transform) and LC-SLM is a Fourier plane, where the amplitude is being replaced by the specific Gaussian profiles and limited by the projected fiber NA at the same time.

VS construction, it is not necessary to determine the distance of the object to be propagated and the distance of the resulting image in the simulations.

The PIMs [5] of the fiber were calculated, see the characteristic equation 1.3 [5] and used as input and output basis for the creation of the T. The image of a perfect point propagated through the T was then Fourier-transformed resulting in spatial spectra in Fourier plane. Here, the light pattern was modulated in the following manner.

Assuming that the LC-SLM is a phase modulator, the information about the phase transmission Φ_{out} could be preserved and applied as a pattern on the LC-SLM. The amplitude information was replaced with a specific Gaussian profile and truncated by the size of the projected fiber NA.

Once the spatial light modulation was performed, the complex field was inverse fast Fourier transformed and propagated through the conjugated T. All the procedure of point propagation then resulted in a diffraction limited focal spot at the distal end of the fiber.

Parameters of simulated components

The following parameters were used in the simulation: the fiber aperture radius $a = 25\,\mu\text{m}$, numerical aperture $NA = 0.22$, wavelength $\lambda = 0.532\,\mu\text{m}$. The main sampling N_{grid} of the input and output fields (the basis of the transmission matrix) was 200 pixels. Usually, for the FFT, the sampling of power 2 is used for easier factorisation for the transform. Since MATLAB can work with different sampling equally efficiently this condition was left from consideration. The resulting transmission matrix then had a size of N_{grid}^2 by N_{grid}^2 pixels.

Structure of the simulation

For simulation of focusing, fifteen Gaussian profiles of a different beam-waist were applied, see fig. 1.11. Each time the beam-waist was related to the fiber NA and

expressed by the *OF*, see equation 1.19. The *PR* was then assessed for the representative set of foci for each *OF* and registered. The representative set of foci consisted of 20 focal spots per *OF* and the mean value of their *PR*s was plotted, see the fig. 3.5. The deviation in values of *PR* is presumably caused by intensity oscillation across the fiber core, later referred as circular intensity artefact (fringes) in a section 4.1.1[2]. Since each tested point was captured at a different position in the core region, in a pattern shown in fig. 3.2, its shape and intensity were affected by the imaging properties of different part of the core region. This may cause a highly pronounced asymmetry of point intensity distribution, and therefore, the contribution of background to the *PR* increases.

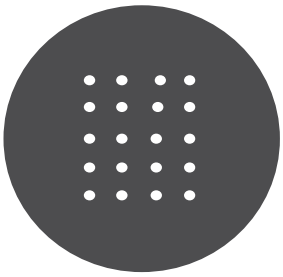

Figure 3.2: Pattern of the points distribution across the fiber core for acquiring the representative set of foci. Each white spot represent the position of one of the 20 points used for calculations.

Evaluation

The main information to be obtained from the simulated data is evidence of any dependence of the focusing quality on the degree of beam truncation. If any dependence was found, it would mean that the MMF is not a completely randomly propagating medium.

There is a suitable method to characterize the focusing ability, the assessment of the *PR*. For evaluation of *PR*, the field fitting was employed. A special function $F(a,w,A;x,y)$ was designed:

$$F(a,w,A;x,y) = A|\mathrm{FT}(G(a,w,A;x,y) + f(x,y))P_{NA}(x,y)|^2. \tag{3.1}$$

The parameters such as fiber aperture a, the beam waist w, transversal location of the maximum x,y and central peak amplitude A of the focal spot were adjusted each attempt of fitting, see fig. 3.3. As a part of the function $F(a,w,A;x,y)$, there was calculated a Gaussian profile $G(a,w,A;x,y)$:

$$G(a,w,A;x,y) = \exp\left(-\left[\left(\frac{a}{w}\right)r(x,y)\right]^2\right), \tag{3.2}$$

[2]The origin of this intensity fluctuation is not clearly explained yet, but the same feature could be observed in experimental MMF imaging.

where $r(x,y)$ represents radius of limiting aperture in **k**-space and is given by: $r = R(x,y)/NA$. The $R(x,y)$ is set of the coordinates of the field. The tilt of the field $f(x,y)$ corresponds to:

$$f(x,y) = 2\pi i(x+y)^2, \tag{3.3}$$

and the limiting projected aperture $P_{NA}(x,y)$ is given by:

$$P_{NA}(x,y) = \exp\left(-r(x,y)^M\right), \tag{3.4}$$

where M is a high number for definition of circular shape of the projected numerical aperture.

The ratio of the intensity-sum of the fitted profile to the intensity-sum of the simulated data provides the PR values.

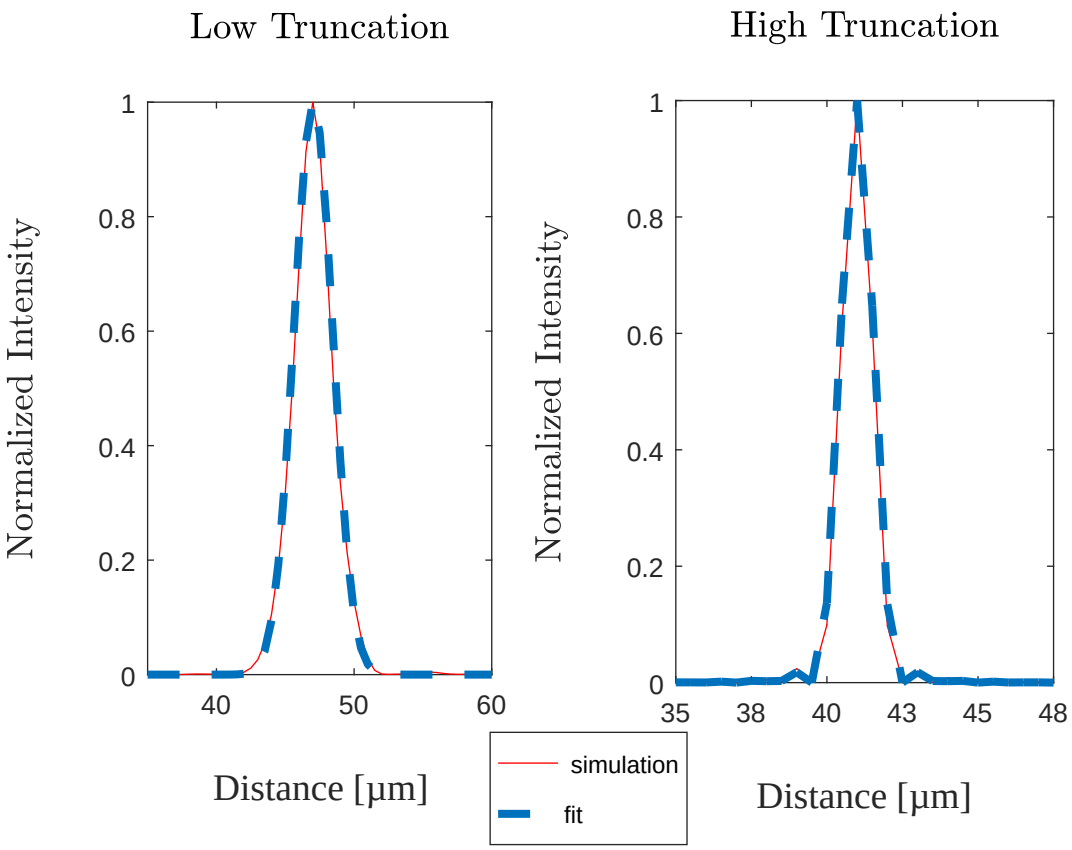

Figure 3.3: Cross section of the data (red) and fitted function (blue). The left figure shows the result for a low truncated beam and on the right figure a high truncated beam can be seen.

Another aspect evaluated for simulated data was the peak-width of the focal spots, see fig. 3.4. The peak diameter provide the information about the appearance of a pointlike object resolved by optical system. Therefore it is an important criterion which gives an additional information about the resolution ability. The full width is measured in a half-height intensity of the peak, therefore it is called a full-width-half-maximum (FWHM). Here, the MATLAB function @findpeaks was employed rather than reading the peak width directly from the fitted function $F(a,w,A;x,y)$ due to its simplicity.

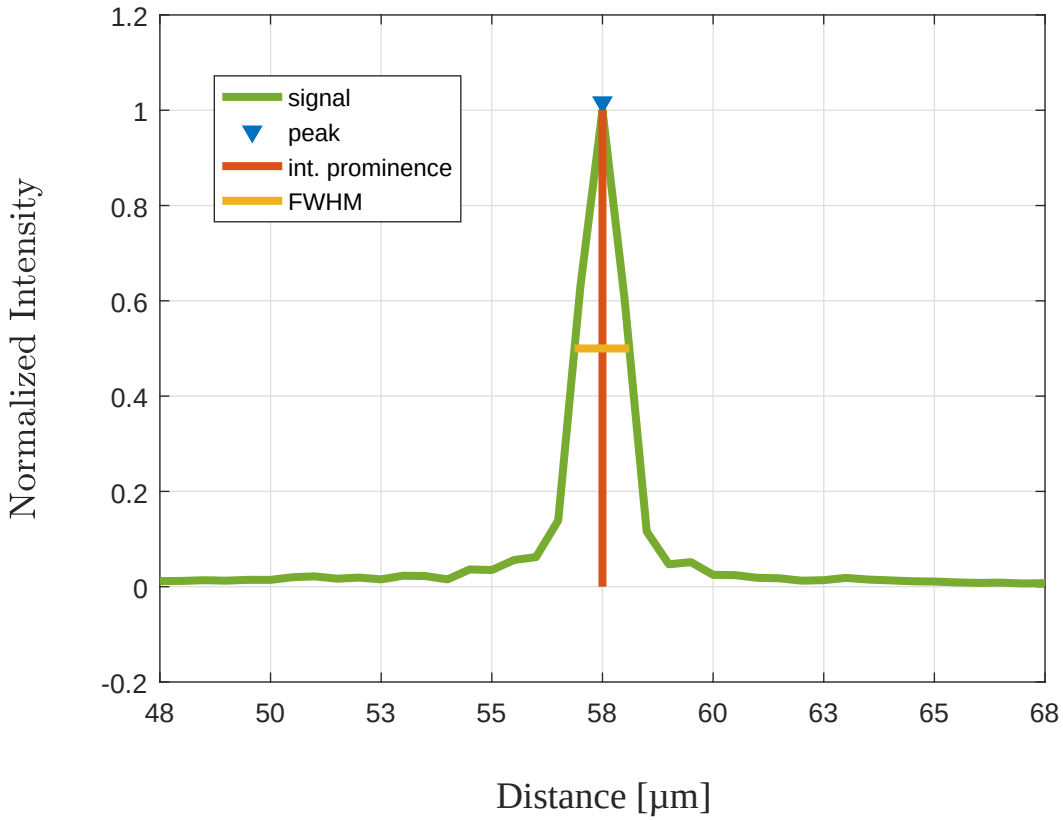

Figure 3.4: Focal spots width measurement.

3.1.2 Summary

By evaluation of the simulated data, presented in figs. 3.5 and 3.6, it was shown that there is a strong influence of illumination on the MMF optical system performance.

The trend of *PR* behaviour is presented in fig. 3.5, where the grey line shows a theoretical limit of *PR* mean values for phase-only modulation performed in random media ($\approx 78\%$), explained in section 1.2.2. The conclusions of previous studies regarding the phase modulation [7], would argue that the *PR* for all types of illumination should be approaching the above-mentioned theoretical limit of $\pi/4$. However, here it is shown that it is possible to achieve even higher values than the theoretical limit for random media is. This means that the light propagation in MMF is not completely random and depends on a specific external conditions, such as illumination overfilling factor of fiber *NA*.

The highest *PR* values appeared for the *OF* around 50%, which has also the smallest deviation from the mean *PR* value. For the peak-width measurement, the width is decreasing with increasing *OF*, approaching the considerably low values for *OF*s 70% and higher.

In the following part this theoretical prediction will be supported by the experimental measurements.

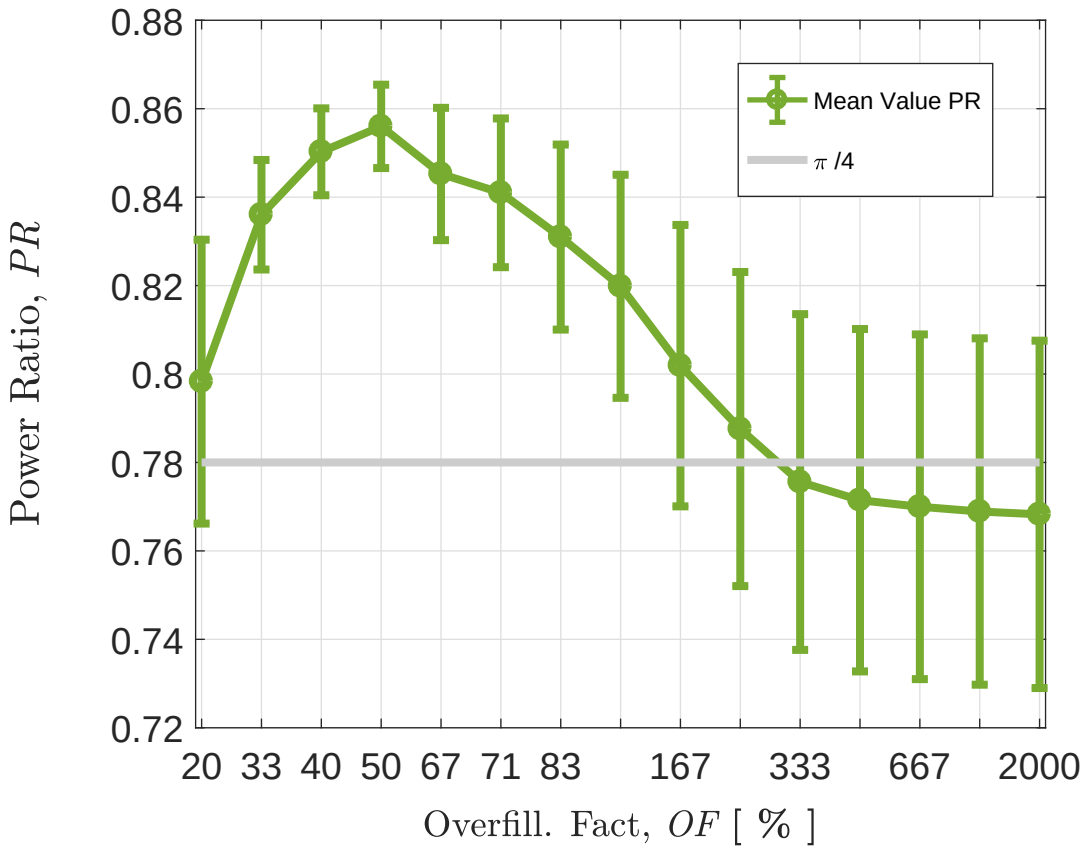

Figure 3.5: Mean power ratio. The simulated data were assessed by field fit. The grey line presents a theoretically predicted limit for PR of the optical system containing random media and using the phase-only modulation ($\pi/4 \approx 78\%$). For each OF, twenty focal points in different position were tested. The data points are represented by green dots and the green solid line is a guide to the eye.

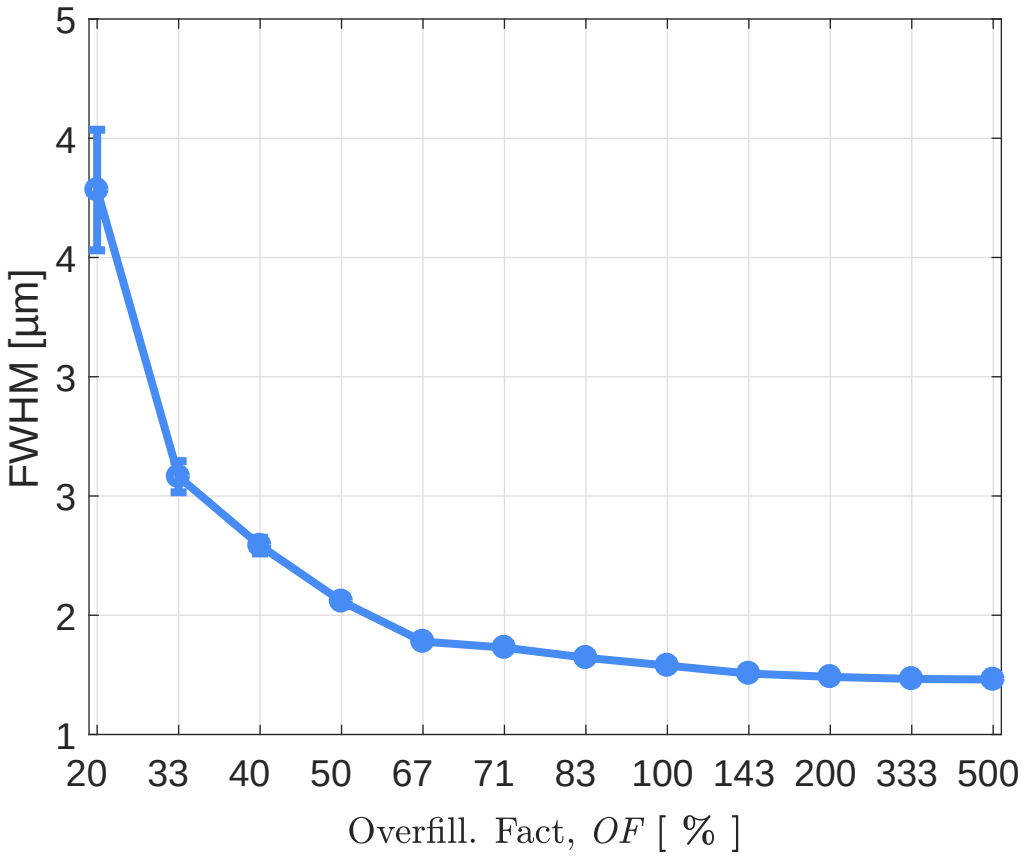

Figure 3.6: FWHM of foci. The full-width-half-maximum was analysed for twenty foci and for each OF. The data points are represented by blue dots and the blue solid line is a guide to the eye.

.

3.2 Experiment

The experimental part of this diploma thesis is aimed to verify the previously simulated phenomena. Focal points have been displayed by beams of specific *OF*s. The data were later evaluated by the *PR* method and by assessment of the FWHM of the peak. The result of this experiment will be the evaluation of light propagation through the MMF in dependence on the external conditions of the illumination beam.

I built the experimental optical set-up at the University of Dundee in research group of prof. Tomáš Čižmár as a part of Erasmus+ project. The optical set-up was designed for light transmission through MMF and focal spot projection on a CCD chip.

3.2.1 Methods

The Gaussian profiles with different *OF*s were processed by the additional LC-SLM. Therefore, the experimental set-up spit into two main parts. The first part, containing the LC-SLM for the Gaussian profiles purpose and the second part with the LC-SLM for the purpose of the T acquisition.

A separate calibration of the first part of the set-up (from the laser source to the LC-SLM$_1$) was applied. The SLM masks were designed to deflect the signal into the first diffraction order of a grating applied and concentrate the light to the shape of the Gaussian beams with different beam-waists. In table 3.1 the representative examples of diffraction masks are shown.

Table 3.1: Difraction masks applied on the first LC-SLM. The masks compensate for optical aberrations of preceding optical components and shape the beam to the Gaussian profile simultaneously.

OF [%]	20	30	50	200
SLM masks	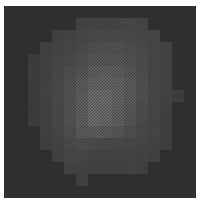	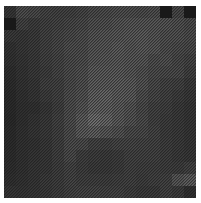		

The second part of the set-up contained the MMF and it was calibrated for the MMF each time before acquiring particular dataset. The dataset comprised nineteen focal points per each *OF*. Every focal spot was imaged by three pictures for three different exposure times, shown in table 3.2, to extend the camera dynamic range. The three images were combined to one image with high number of grey levels.

The analysis of the data was using the same fitting procedure as in the case of the first simulation. The sum of real-data intensity and a sum of fitted field were compared and the *PR*s were registered into a graph shown in fig. 3.9. A representative number

Table 3.2: Capture of three different exposure times of one focal spot.

Exposure time [ms]	1	10	100
Recorded intensity	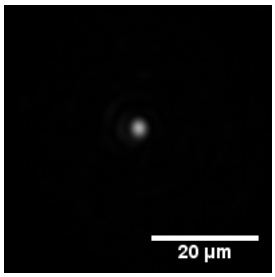	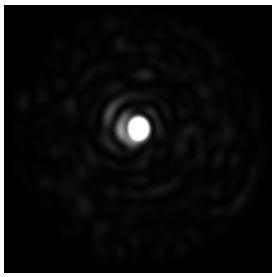	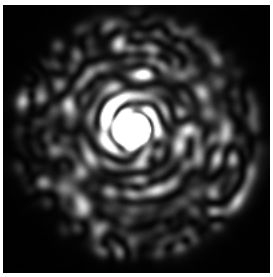

of datasets are analysed and plotted, since the data sets did not vary significantly in the intensity.

3.2.2 Experimental set-up

The schematic illustration of the experimental set-up is shown in fig. 3.7 and a photo of the real experimental set-up can be seen in fig. 3.8.

The MMF used in the experiment was 5 cm long step-index MMF of $NA = 0.22$ (Thorlabs FG050UGA) and refractive indeces $n_c \approx 1.456$ (core: Pure Silica) and $n_{clad} \approx 1.450$ (cladding: Fluorine-Doped Silica) were employed. Due to the small refractive indeces difference the fiber could be considered as a weakly guiding fiber. For the used wavelength of $\lambda = 1064\,\text{nm}$ (LASER CrystaLaser CL1064-3W0) the number of modes for this MMF is approximately 200. The wavelength is two times higher than the wavelength used in simulations. Since the number of modes in the same MMF for higher wavelenght is smaller, the efficiency of phase modulation with the same number of SLM input modes is same or higher (if the phase modulation was insufficient).

From the source, see the top left corner of fig. 3.8, the light is transmitted through the $\lambda/2$ plate HWP (Thorlabs WPH05M-1064), optical isolator, HWP, beam expander comprising two lenses ($f = 30\,\text{mm}$, $f = 150\,\text{mm}$), polarising beam-splitter BS (Thorlabs PBS053), where the reference and the object beam were separated. The reference beam was transmitted through $\lambda/4$ plate QWP (Thorlabs WPQ05M-1064) and coupled by lens ($f = 11\,\text{mm}$) to a singlemode fiber. The signal beam propagated through lens ($f = 150\,\text{mm}$), lens ($f = 200\,\text{mm}$), HWP, to the LC-SLM$_1$ (Meadowlark: HSPDM512), where it was modulated and the Gaussian masks with aberration compensations were applied. The light was focused by a $f = 250\,\text{mm}$ lens, and the first order of the diffraction from the LC-SLM$_1$ was isolated using the iris (Thorlabs SM1D12D). The light was then collimated and sent to the LC-SLM$_2$ (of the same type).

At the LC-SLM$_2$, there was the MMF calibration performed for each measurement, and the first order was then reduced and reflected by two lenses and two mirrors ($f = 150\,\text{mm}$, $f = 100\,\text{mm}$). The light travelled through the QWP and the objec-

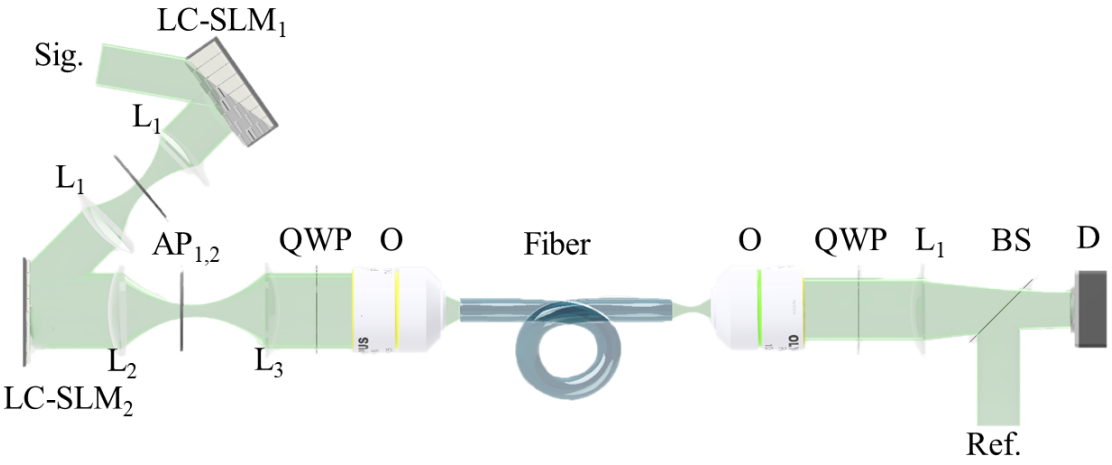

Figure 3.7: The schematic figure of essentials components of the experimental set-up. The figure is originally created for purposes of article [6] by Sergey Turtaev and modified for purpose of this thesis. LC-SLM$_1$, LC-SLM$_2$: Liquid crystal spatial light modulators; AP: iris diaphragms; QWP: quarter-wave plate; MMF: Fiber; O: microscope objectives; L: lenses; BS: beam splitter; CCD: CCD chip; ref: reference beam; sig: signal beam.

tive O (Olympus objective RMS20X - Plan 20x) and focused to the MMF. The light transmitted through the fiber was propagated within another objective O (Olympus objective RMS20X - Plan 20x), with opposite alignment, to the second BS, where it is combined with the reference beam. The beam was imaged with lens ($f = 250\,\mathrm{mm}$) on a CCD chip (Basler pia 640-210gm: 4.7 um pixel size).

All the digital components of the set-up were controlled via LabVIEW interface. The LabVIEW virtual instruments (VIs) for the manipulation with the first LC-SLM were programmed particularly for this experiment. The remaining used VIs were adopted from the database of Complex Photonics group in Dundee and modified for the experiment purposes.

3.2.3 Summary

The measured PR is shown in fig. 3.9. At the experimental data, there can be observed a similar trend as was noticed in the simulation. The PR values increase to its maximal value of $PR \approx 80\%$ for the $OF \approx 40\%$ and then decrease again. For high OFs there can be seen the inclination of the mean PRs to a constant value of $PR \approx 65\%$. However, this value is lower than the theoretical limit of phase modulation. This is probably a consequence of LC-SLMs performance features, described in part 1.2.2 and closely diagnosed in [22, 23]. In the fig. 3.9, there can be seen an unexpected artefact of higher PR values for the $OF \approx 180\%$, this was presumably caused by non-precisely created Gaussian profile at the LC-SLM$_1$. It is also possible to notice a decrease in PR for

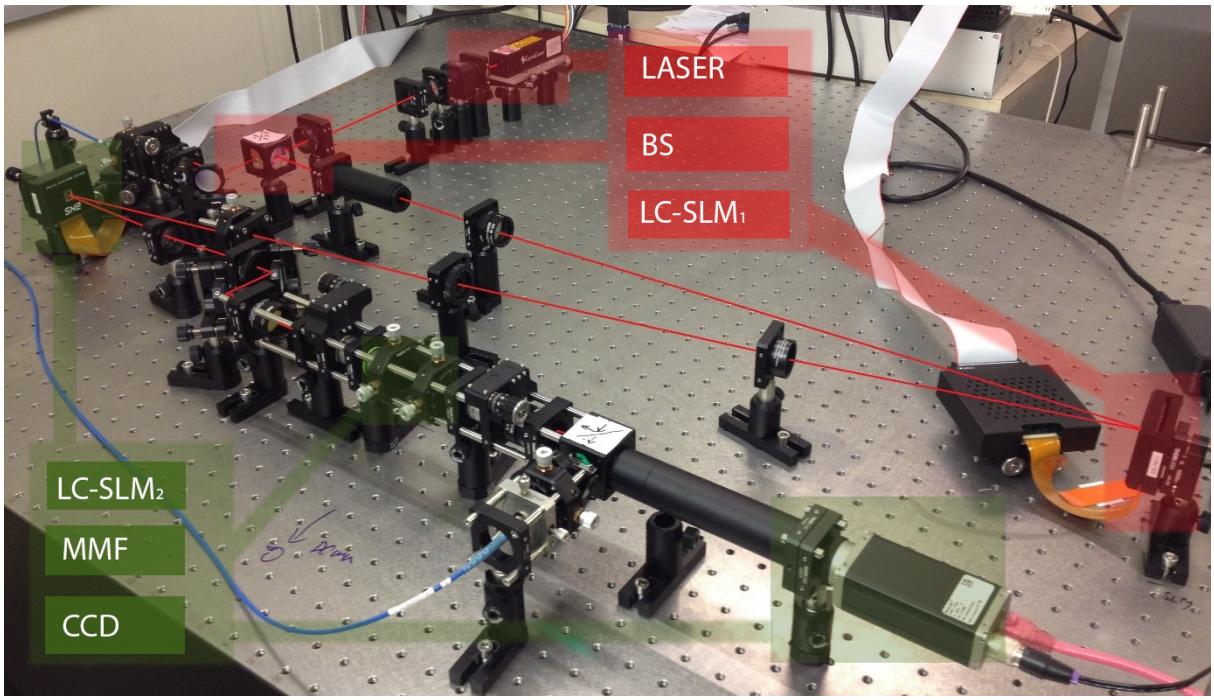

Figure 3.8: Real set-up. The thin red line was drawn to show illustratively the pathway of the transmitted light. The main components (LASER, BS-beam splitter, LC-SLM$_{1,2}$-liquid crystal spatial light modulator, MMF, CCD) are highlighted by red and green colour.

very small values of OF ($\approx 20 - 30\%$). It is most likely due to highlighting of the background for significantly underfilled aperture.

Similarly, as in the case of the first simulation, a significant spread in the data for each OF can be observed. Its origin is presumably the same as that of the simulated data. The uneven transmission caused by the fringes leads to that the side lobes in the data are differently pronounced and the PR varies.

To complete the analysis, the FWHM was evaluated. It can be seen in the fig. 3.10, that the shape and width of the peak differ with the change of OF. The widest peaks are displayed using the least truncated beam. As the OF grows, the range decreases to the lowest measured width, 8 pixels which for our sampling equals 2 µm. The peaks are approaching these values when the SLM is illuminated by Gaussian beam overfilling the projected NA by 60% and more.

Despite the apparent difference in maximum value of the efficiency, the trend of experimental PR behaviour is similar to that of the simulated optical system. The obvious increase in PR is at about $OF \approx 40\%$ for experimental data and 50% for the simulation and thereafter the PR drops to a lower value. The values of FWHM for both, the simulation and experiment, are significantly decreasing for increasing the overfilling factor till the values of OF around 100%. For higher OFs the PR values are reaching the value of lowest measured FWHMs.

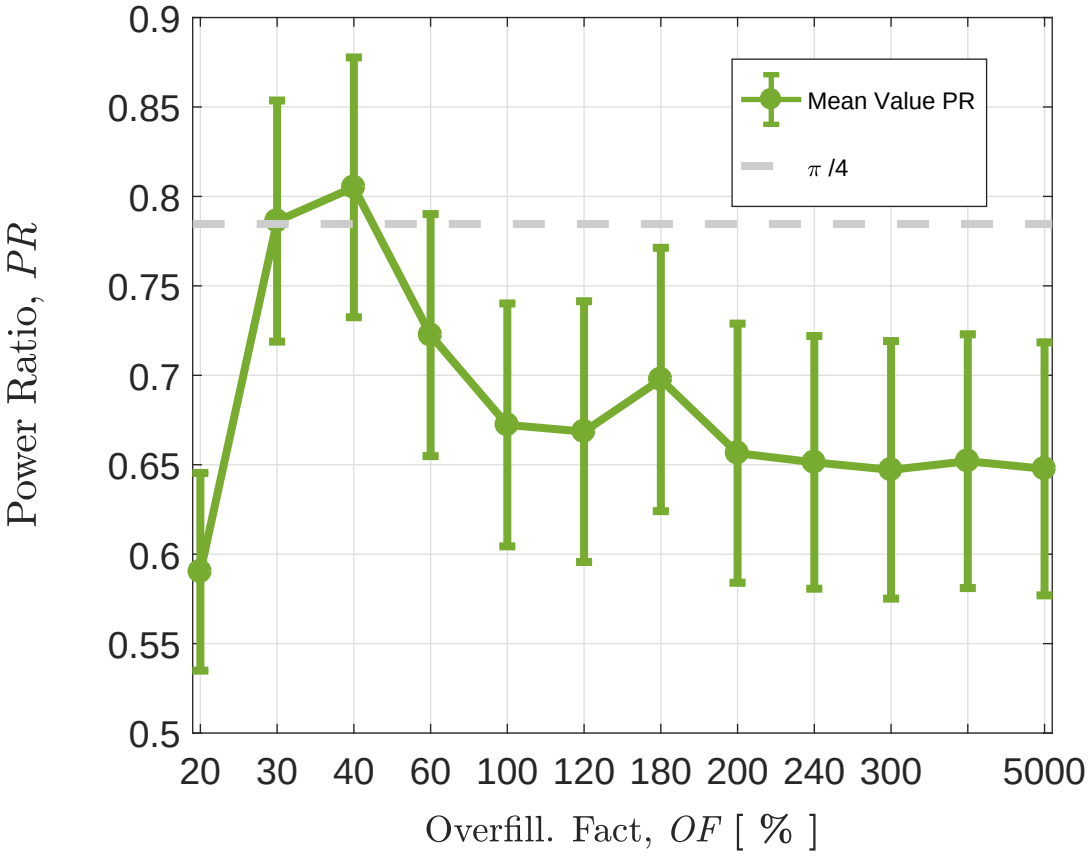

Figure 3.9: Mean power ratio. The experimental measurement of nineteen focal spots for each OF. The grey line shows the theoretical maximum of PR values for phase-only modulation in random media ($\pi/4 \approx 78\%$). The data are represented by green dots and the green line is a guide to the eye.

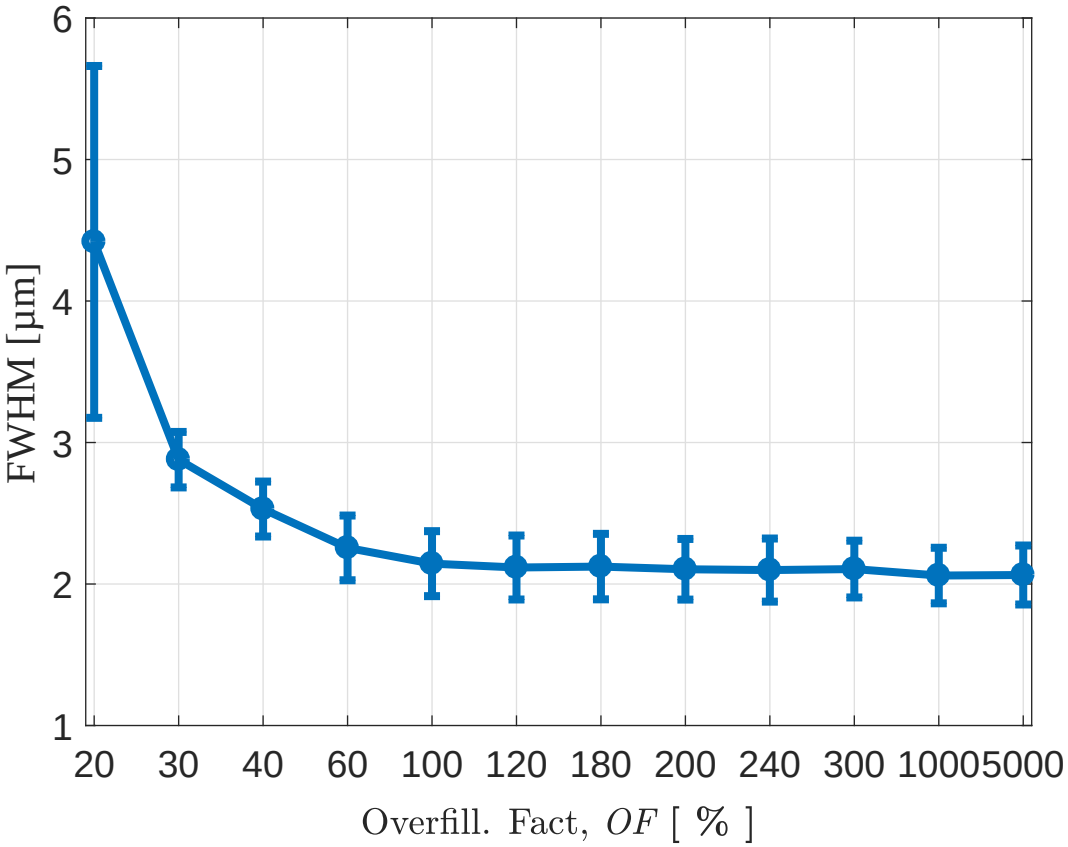

Figure 3.10: FWHM of the peaks was measured for different *OF*s. The data points are represented by blue dots and the blue solid line is a guide to the eye.

4. Limitations of multimode fiber imaging

From the experiment and simulation in section 1.2.1, the following conclusion could be drawn: the performance of the MMF optical system changes with the aperture fill factor. However, the evaluation of MMF imaging quality still need to be evaluated.

This section will focus on examining the limitations of the MMF imaging quality. As the first step, the imaging of specific targets will be simulated. Then the imaging quality of the optical system will be evaluated.

The goal of this section is to find the optimal conditions for MMF imaging, and find the limitations and improvements relative to commonly used illumination of the imaging systems.

4.1 Simulation

The MMF imaging is a scanning imaging technique, therefore the scanning over the distal fiber facet needs to be performed. As it was described in 1.2.1, the transmission matrix was used to transmit the focal spots which were then scanned over the target to be imaged.

At this section the limits of MMF imaging is investigated for OF values ranging from 20% to 1000%. To shorten the calculation time, a representative set of OFs was chosen for each part of the simulation.

The figure " 3 "

The fig. 4.1 shows five representative sets of images that highlight the appearance of the pattern imaged by MMF. As an illustrative example the number three was imaged with each OF. Number three is used mainly because of its structure and the spatial distribution over the fiber core area. In the left part of the fig. 4.1, the SLM plane along with the shape of the applied Gaussian beam and projected fiber aperture is shown. The right part of the sub-figures presents the image of the target imaged using the phase modulation combined with the specific Gaussian beam. All the images were self-normalized.

(a) $OF = 20\%$.

(b) $OF = 50\%$.

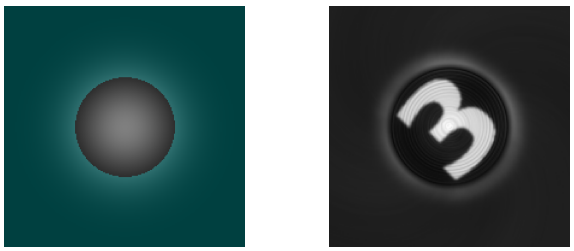

(c) $OF = 100\%$.

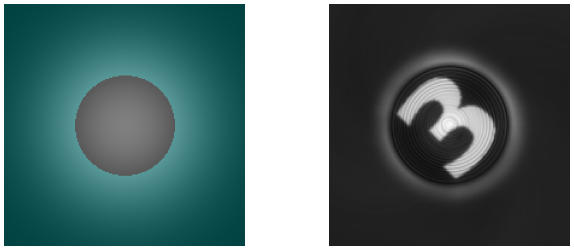

(d) $OF = 167\%$.

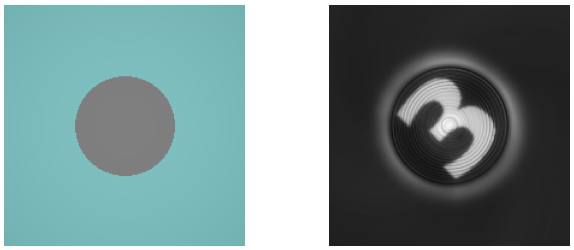

(e) $OF = 1000\%$.

Figure 4.1: Imaging with different beam-waists. Left part of each sub-figure shows the Gaussian beam used for illumination of SLM and coloured truncation mask with the diameter of projected fiber aperture. The right figure shows the result of the target imaged using the phase-only modulation. Each of the images is normalized to its maximal value.

4.1.1 Intensity artefacts

The first examined aspects were the intensity fluctuation artefacts. The two types of intensity fluctuations were found when imaging with the MMF. The first type is a starfish artefact, not interfering with the core region. The second manifested intensity feature was a circular intensity fluctuation over core area.

The starfish artefact (where the bright rays go from the core-cladding interface to the cladding) appeared for small *OF*s, see e.g. fig. 4.3a. The origin of the artefacts is not entirely clear. But the accentuation of the artefact for the small *PR* is caused by image normalization. The intensity of the displayed object is noticeably lower for the small *OF* and the ratio of the background intensity and the displayed object intensity is low. Thus, during normalization both subjects, the observed object and background, are highlighted.

However, more important for the research are the circular artefacts due to their position in the core area. Examined was a pronunciation of unwanted circular intensity variations, here called fringes. The artefacts show up in any case of illumination of SLM and they were observed for imaging of a uniform bright target. For a perfect optical system, this target would be displayed with a uniform intensity. However, when imaging by MMF, quite pronounced intensity inequalities over core area appeared. The significance and properties of the artefact were measured by the following method:

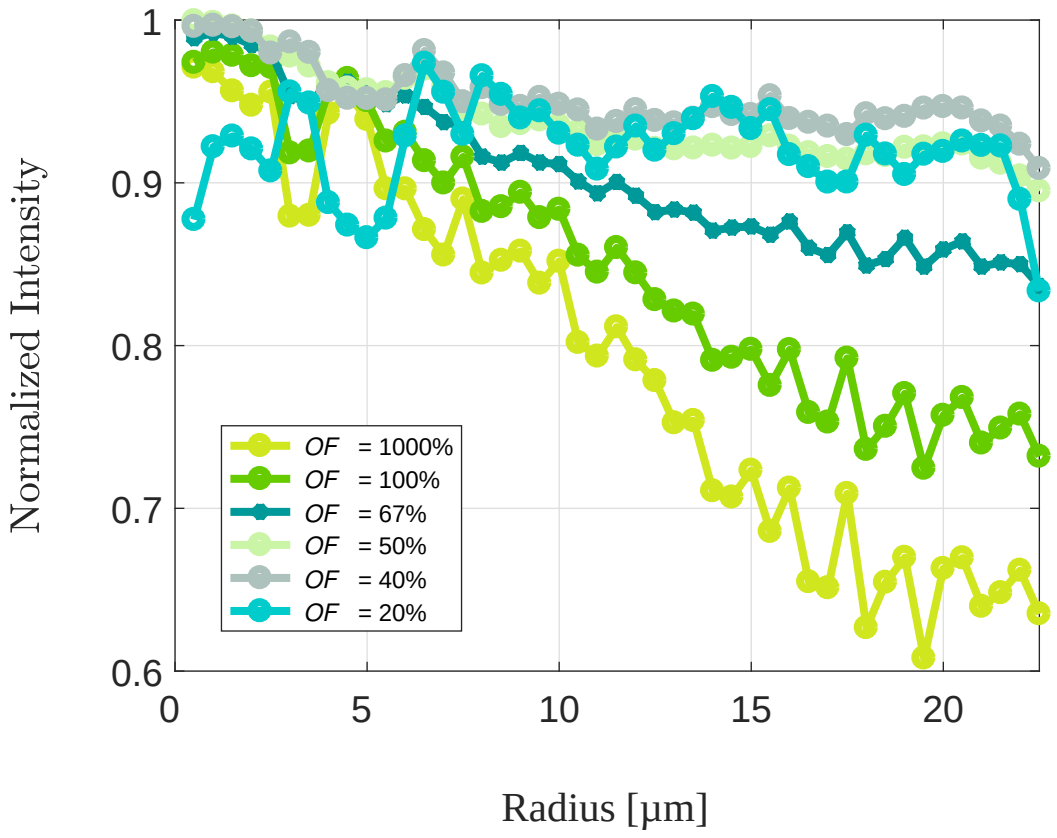

Figure 4.2: The intensity variation across the fiber core area. The image of an uniform bright target divided into concentric circles of a given radius with normalized intensity-values. The data points are represented by coloured dots and the solid lines are guides to the eye.

The images were self-normalized and divided into concentric circles, for which the mean value of intensity was calculated. The fig. 4.2 shows the mean values of normalized intensity as a function of an image radius. For clarity, the curves are presented without error bars. The fig. 4.3 shows the pattern observed at the image and the mean values of the intensity for 4 selected OFs. Evidently, there can be observed a trend of decreasing intensity with increasing distance from the centre of the fiber core for all except very low OFs. This phenomenon is likely to play a significant role in displaying structures, such as SFs targets for MTF calculation. Therefore, it is difficult to accurately assess the MTF for specific frequencies, when the contrast and intensity are probably in a relation with the position to the imaging device.

In fig. 4.3, the deviation of the intensity is expressed by error-bars and it is evidently lowest for slightly underfilled aperture, $OF \approx 50\%$. For this overfilling factor the overall core intensity is the highest.

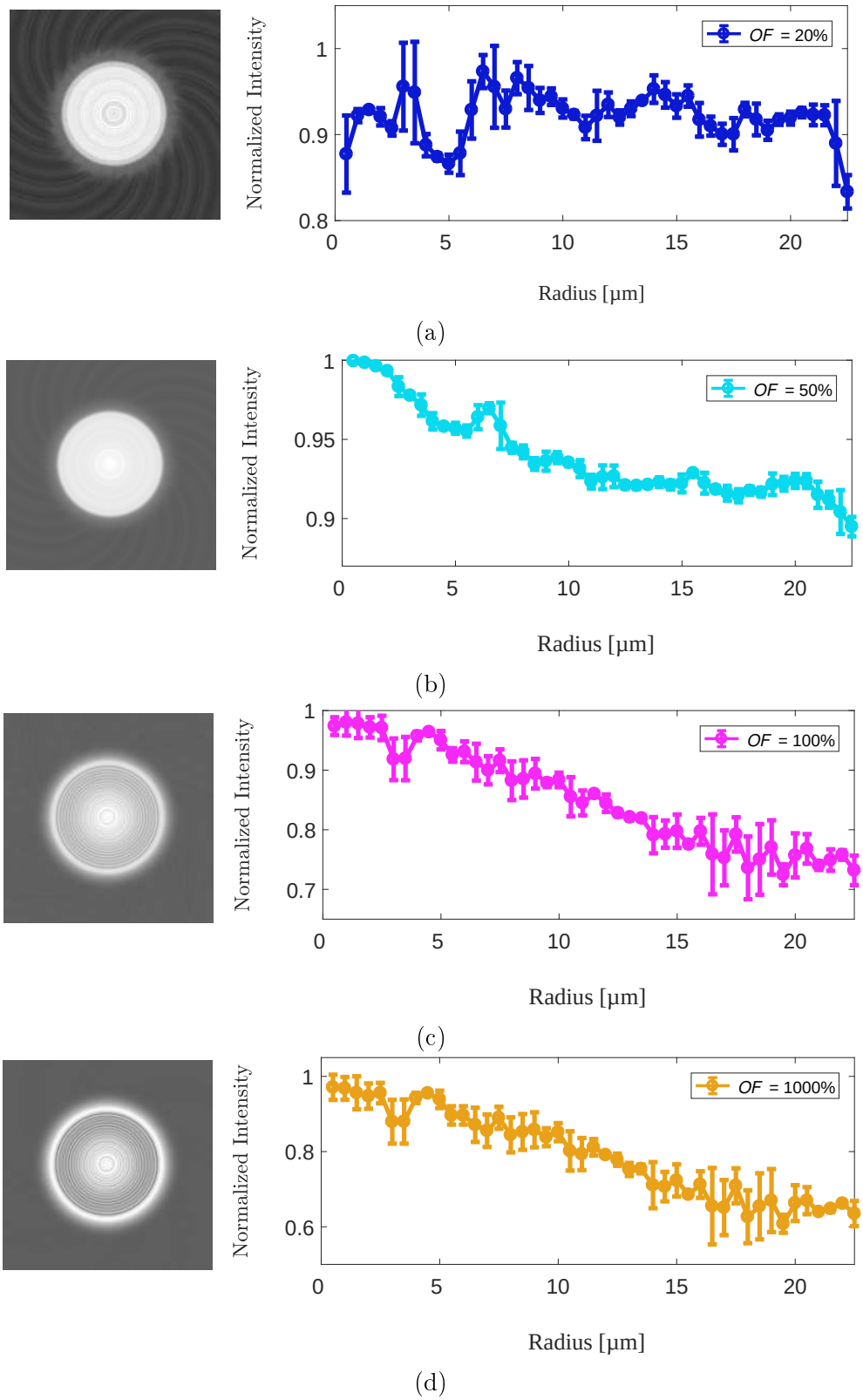

Figure 4.3: The pronunciation of circular intensity artefact. At the left column there are intensity patterns of a image of unitary bright target. The plots at the right column show the calculated mean values of intensity. The data are shown for *OF*s 20%, 50%, 100% and 1000% respectively. The radius is measured in the image. The data points are represented by the coloured dots and the solid lines are guides to the eye.

Table 4.1: Targets for MTF measurement. For illustration the circular fiber aperture is added.

Cycles per core-diameter	1	2	3	5	8	15
Target	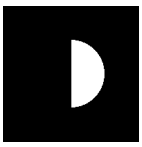					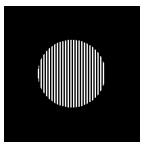

4.1.2 Modulation transfer function

The most convenient characteristic of an imaging system is the MTF which characterize the ability of the contrast transmission and describes the spatial resolution of the system. For this diploma thesis the targets shown in table 4.1 were imaged by each *OF* and the images were later analysed by MTF. The displayed samples consist of several binary bars and form a structure with a clearly defined spatial frequency. Each frequency was displayed separately. The contrast was calculated by image intensity summing in the direction of the imaged structure, analysing the maxima and minima of the imaged structure and applied in equation 1.17. The MTF was then plotted in fig. 4.4 as a function of the displayed spatial frequency.

Other attempts were made to evaluate the contrast, but the contrast in the complex media is influenced by the location of the analysed area in the resulting image and the relative position of the target to be imaged and the imaging optical system [31]. Three main methods of contrast evaluation were applied: the subtraction of histogram values, the convolution of the image with a special filter and integration of the image in the direction of the displayed structure. The most conservative method of summing the picture was then chosen for its reliability. Image filtering using the convolution filter has proven to have an excessive influence on the resulting image contrast, and has significantly impacted the influence of fringes. Therefore, the MTF values did not match reality when using this method and the contrast was higher than the one observed in original images. The reading of the histogram values also proved to be inappropriate for the given analysis because of the fringes existence. It significantly deteriorated the contrast subtracting reliability.

An improvement of MTF plays a significant role in imaging quality. It is clearly seen in fig. 4.4, that using different *OF*s results in a large difference in MTF, therefore in the performance of imaging. For a perfect optical system, the contrast transmission function would be constant for all SFs. This deduces that the best performing systems are those that provide the highest MTF values for imaging of the highest SFs. In fig. 4.4, there can be seen a comparison of MTFs for the representative values of *OF*s.

The contrast transmission was of comparable quality for all *OF*s in low SFs, but a

significant difference appeared for displaying of detailed structures. The most noticeable is the decrease in the contrast transmission quality for the highly underfilled NA. For $OF = 20\%$, we see a perceptible drop in MTF values with increasing of SFs. It is possible to verify the fact in table 4.2, where the decrease to contrast is noticeable by the naked eye. In the fig. 4.4, it is shown that MTFs reach higher values for higher OFs, but best for $OF = 50\%$. It is very likely that this fact is caused by the above-mentioned appearance of fringes. For $OF = 50\%$, the fringes were much less pronounced than for other overfill factors.

According to the MTF measurement, the best preforming OF is $OF = 50\%$. When comparing the fig. 4.4 and the cross sections of the images in table 4.2, there can be seen an interference of fringes and imaged structure in table 4.2. The most noticeable is the phenomenon for high SFs imaged with a highly overfilled aperture. The phenomenon also occurs when the contrast is subtracted and presumably causes lower values of MTF for high OFs, see fig. 4.4.

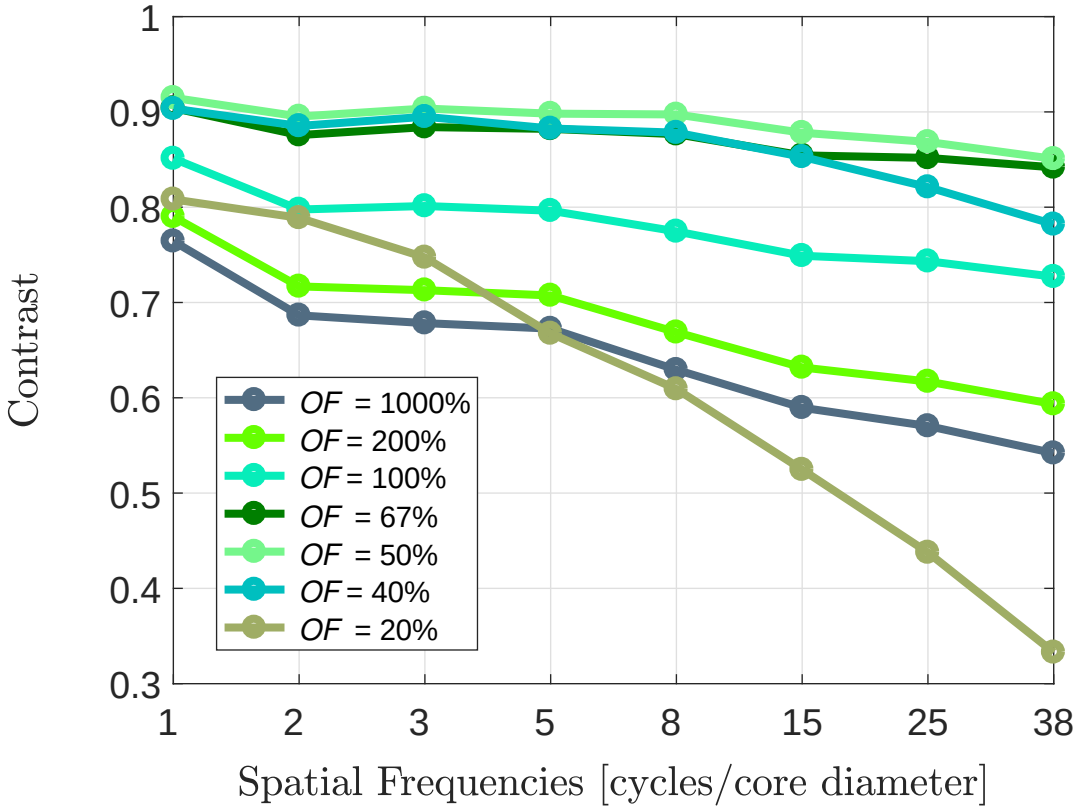

Figure 4.4: Modulation transfer function of seven different Gaussian beams. The data points are represented by coloured dots and the solid lines are guides to the eye.

4.1.3 Resolution

To determine the resolving ability of the MMF, the target was changed to two diverging points. The degree of detachment of both points was observed in the resulting image. As mentioned in part 1.2.3, for this diploma thesis the Rayleigh criterion of separation was selected.

Table 4.2: Spatial frequencies imaging. The trimmed images of transmission of different spatial frequencies. Each column shows an image of specific SF for six different *OF*s.

OF	1 [cyc/core]	2 [cyc/core]	3 [cyc/core]
1000%			
100%			
67%			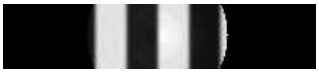
50%			
40%			
20%			
OF	5 [cyc/core]	10 [cyc/core]	25 [cyc/core]
1000%			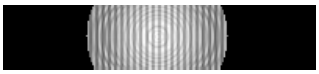
100%	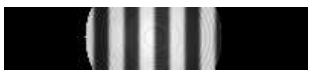		
67%			
50%			
40%			
20%			

Here, MATLAB function @findpeaks was used to evaluate the peak intensity prominence, see fig. 4.5. Parameters of peaks obtained by this function were then inserted in the equation 1.16. The depth of modulation δ was calculated by above-mentioned equation and the results were registered in the fig. 4.6. The resolvable limit is set at 20% of modulation depth according to Rayleigh criterion.

It is obvious, that for the more truncated beams the resolving capacity is significantly higher than of the low *OF*s, see fig. 4.6. For wider peaks appearing when using less truncated beams, the resolution is considerably worse. To create a clearer idea of a system behaviour, the cross sectioning charts of resulting images are incorporated, see fig. 4.7.

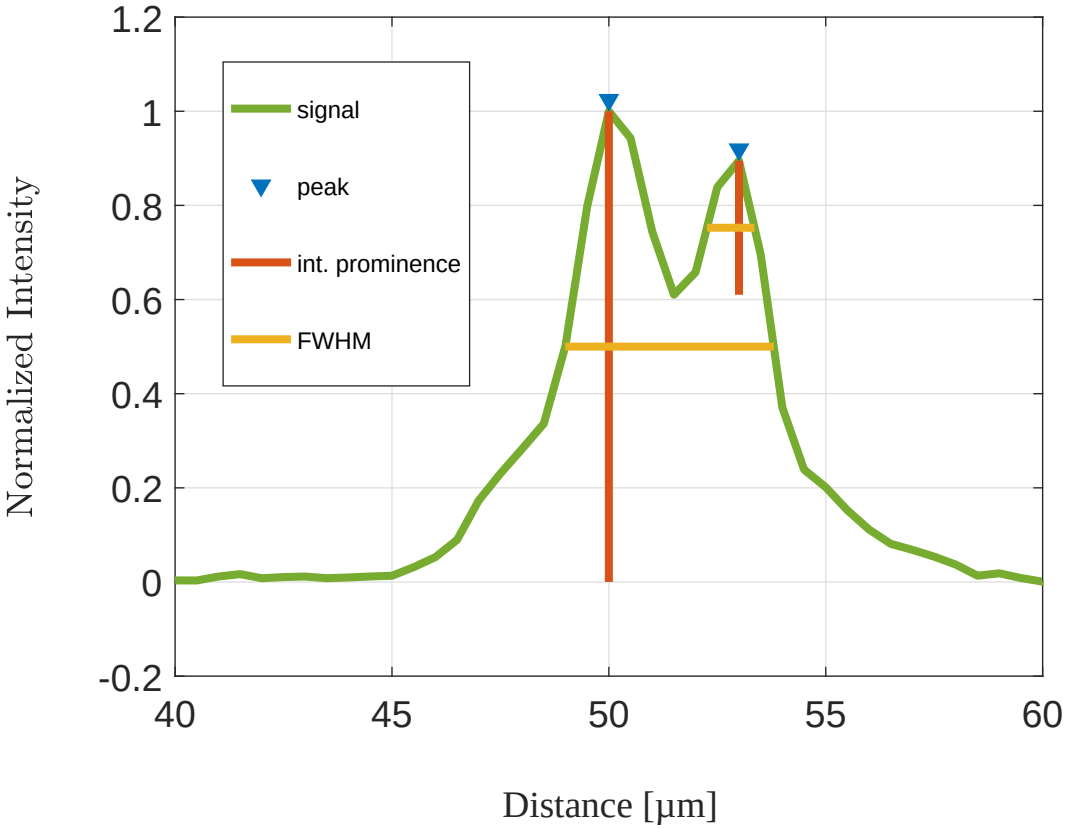

Figure 4.5: Resolution of two points with 2 pixel distance in a target to be imaged. The x axis shows the distance in µm at the resulting image.

From the figures in 4.7 a clear trend can be drawn, when the resolution of the two receding points improves with the degree of aperture filling and the beam truncation. The graphs in fig. 4.7 show the difference of peak shapes when displayed with different *OF*s. At first glance, it is obvious that the resolution is the highest for *OF*s around 1000%.

The resolution is highest when the beam is highly overfilling the projected fiber aperture. However, when imaging a complex structure or a structure with bright background the contrast transmission is influenced by the pronunciation of the fringes. This means that if we scan with the MMF imaging technique across a field with a very bright background, the contribution of the background impede the ability to transmit the contrast. Therefore, to select the type of illumination, it is necessary to consider

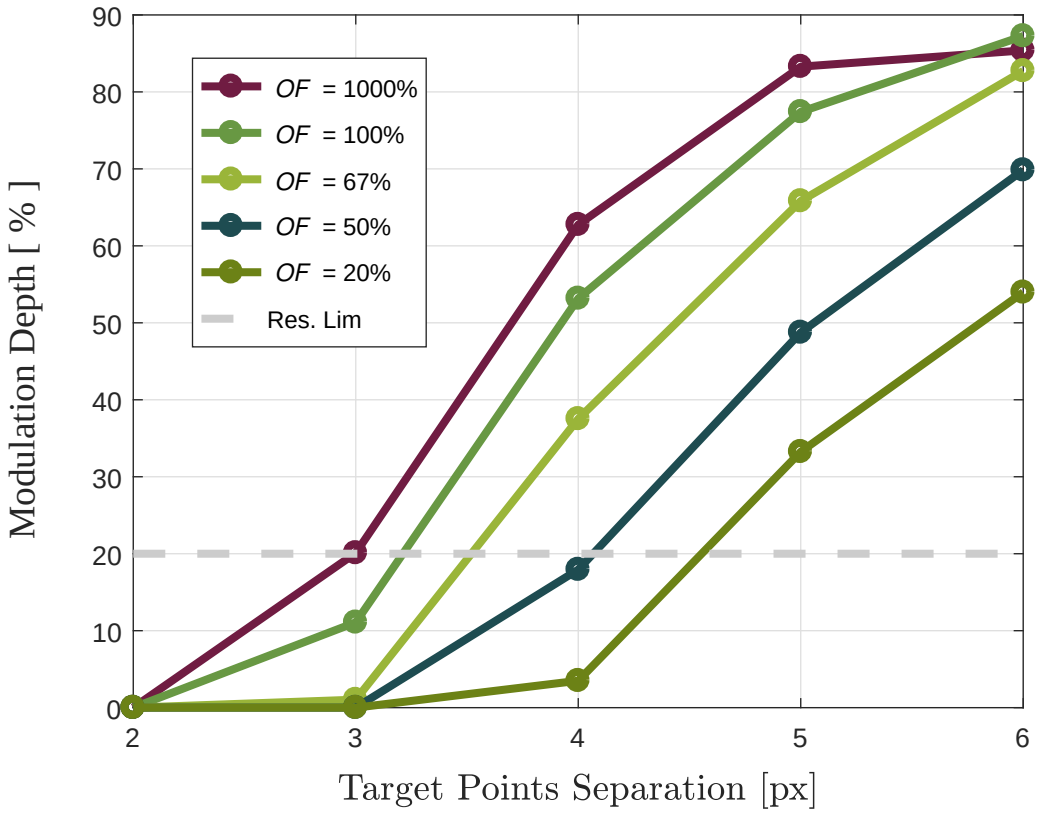

Figure 4.6: Modulation depth of of two pointlike objects. The separation of the point at the target was 2, 3, 4, 5, and 6 pixels, respectively. Five representative Gaussian profiles were examined for this parameter. The modulation depth gives information of the resolution ability of two separate points. For modulation depth over 20% the points are able to be resolved by the optical system.

the purpose of the imaging and the environment in which we will be operating. For example, for in-vivo microscopy, if the sample bright, imaging quality can deteriorate for the more overfilled fiber apertures, and a change of the illumination conditions should be considered.

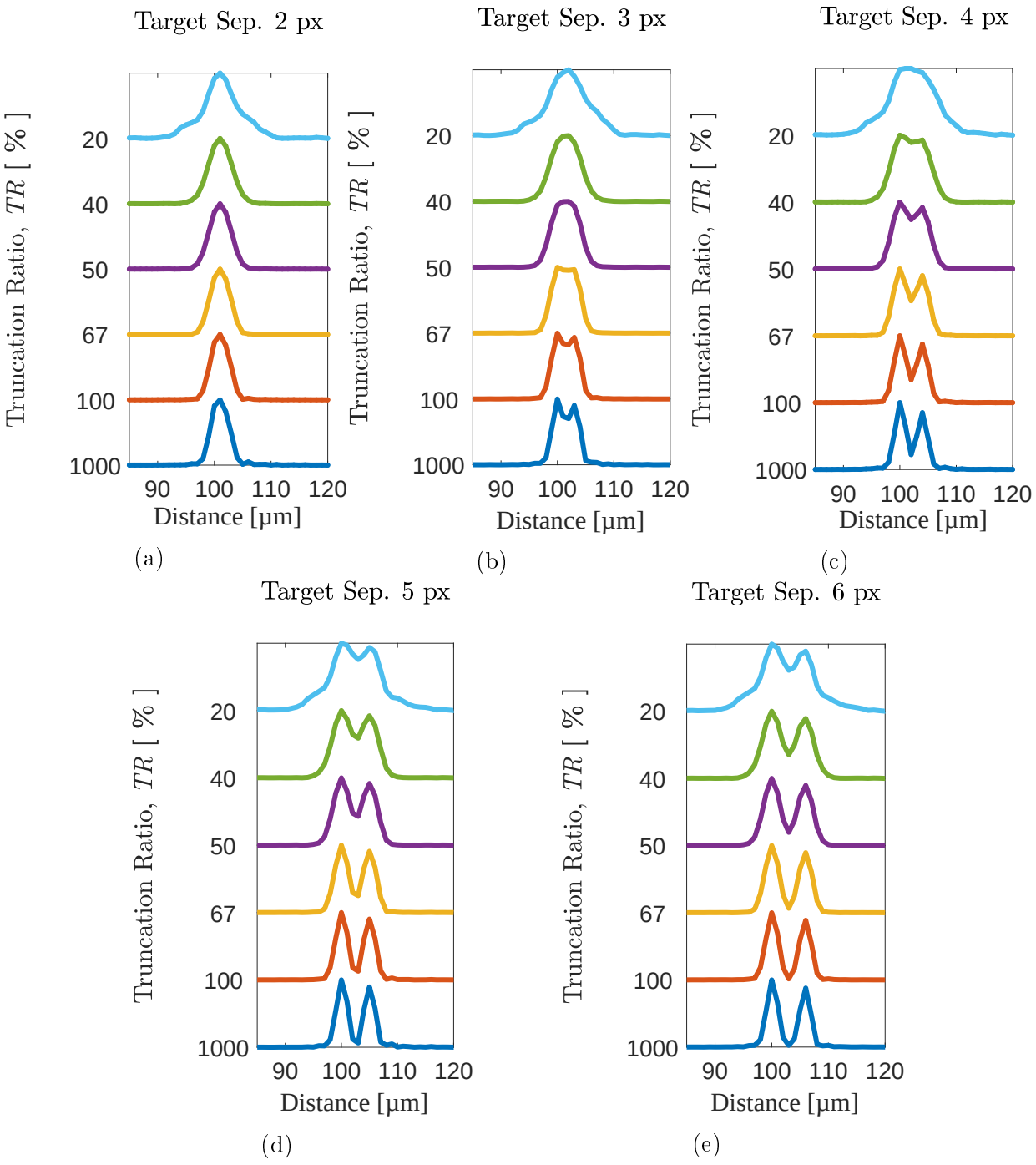

Figure 4.7: The cross sections of image of two separate pointlike objects. Each subfigure shows different points to be imaged separation for six representative *OF*s.

4.2 Discussion

For a clear interpretation of the data, it is necessary to combine all the above-mentioned parameters at once. Obviously, some methods of analysis appeared to have a difference in the trend. But the result of all analyses: *PR*, FWHM, MTF, circular intensity artefacts and resolution separately refer how is the efficiency of the optical system influenced by the illumination overfill factor.

The assessment of the imaging quality is closely connected to what we prefer from the criteria. Assuming resolution as the most important parameter, the highly overfilled aperture (*OF* around 1000%) appears to be the most appropriate one. The two pointlike objects for this overfilling factor are perfectly resolved while objects imaged with the underfilled aperture are still under the resolvable minimum.

The MTF analysis shows good results for all *OF*s when imaging low SFs. However, when higher SFs are imaged, the differences between *OF*s appear. The interactions between imaged structures and intensity artefacts, fringes, also emerge. Therefore, when assessing the contrast transmission ability, fringes play a significant role. The most balanced intensity values across the fiber core area appear for *OF*s reaching 40% to 50%. And the highest MTF values for high SFs are performed by $OF = 50\%$.

From all of the above-mentioned facts, the following conclusions can be drawn. MMF is often considered a random medium, but in this work we see that the fiber changes its focusing and imaging properties depending on the change of illumination. Therefore, it is obvious that the fibers can not be regarded as completely random scattering media.

Conclusion

This thesis presents a new improvement for MMF imaging and discusses its limits. There has been presented a phenomenon of MMF light propagation dependence on a change of external conditions for imaging, such as illumination overfilling factor. The computer simulations and the experiment were introduced.

The algorithms presented here have been constructed as MATLAB simulations of optical waves behaviour when propagating within the MMF. A light propagation supposed to show how the performance of the imaging is limited. The principles of digital spatial light modulation were applied for the MMF light propagation. Firstly, the ability to focus the available power to the focal spot was simulated and later experimentally measured. Further, the properties of the scanning point were examined. As the last step, specific targets were displayed with the system and analysed.

It is demonstrated, hereby, that the degree of overfilling the fiber aperture has a significant effect on the transmission of information through the MMF optical system. From this fact it can be deduced that the MMF is not a completely random medium, but it shows signs of dependability on the setting of external conditions. It has also been indicated that it is necessary to choose the preferred criterion in the assessment of the imaging quality and, accordingly, to take another step further.

To summarize the work, the goals of this thesis were fulfilled. The specific limits for the multimode optical fiber imaging were found and the underlying theory was provided. The computer simulations of the phenomena were carried out and the experiment was performed to conform one of the simulations. Finally, the data were analysed and the conclusion for each evaluation criterion was drawn.

In this work several aspect of MMF imaging and focusing characteristics were shown and some of them can be the topic of a future work. The next step to be taken is to experimentally verify the results of the second simulation. The optical set-up will be designed to image specific structures so that the intensity artefacts and the imaging quality can be evaluated. The demonstrated approach could be further applied in optical devices employed in medical practise for in-vivo micro imaging.

Bibliography

[1] GORDON, G. S. D. et al.: Single-Pixel Phase-Corrected Fiber Bundle Endomicroscopy With Lensless Focussing Capability. *JOURNAL OF LIGHTWAVE TECHNOLOGY*, vol. 2015, no. 33, 2015: pp. 3419–3425, Available from: doi:10.1109/JLT.2015.2436816.

[2] ČIŽMÁR, T. DHOLAKIA, K.: Shaping the light transmission through a multimode optical fibre. *Optics Express*, vol. 2011, no. Vol.19, 2011: pp. 18871–18884, Available from: doi:10.1364/OE.19.018871.

[3] CHIANG, H.-P., CHANG, W.-S. WANG, J.: Imaging through random scattering media by using cw broadband interferometry. *Optics Letters*, vol. 1993, no. Vol. 18, 1993: pp. 546–548, Available from: doi:10.1364/OL.18.000546.

[4] SNYDER, A. W. LOVE, J. D.: *Optical waveguide theory*. London: Chapman & Hall, first edition, 1983, ISBN 0-412-24250-8.

[5] GLOGE, D.: Weakly Guiding Fibers. *Applied Optics*, vol. 1971, no. Vol.10, 1971: pp. 2252–2258, Available from: doi:10.1364/AO.10.002252.

[6] TURTAEV, S. et al.: Comparison of nematic liquid-crystal and DMD based spatial light modulation in complex photonics. *Optics Express*, vol. 2017, no. Vol. 25, 2017: pp. 29874–29884, Available from: doi:10.1364/OE.25.029874.

[7] POPOFF, S. M. et al.: Controlling light through optical disordered media. *New Journal of Physics*, vol. 2011, no. 13, 2011: pp. 1–26, Available from: doi:10.1088/1367-2630/13/12/123021.

[8] LOTERIE, D. C.-M.: Microscopy and digital light shaping through optical fibers. 2017.

[9] POPOFF, S. et al.: Image transmission through an opaque material. *Nature Communications*, vol. 2010, no. 1, 2010: pp. 1–5, Available from: doi:10.1038/ncomms1078.

[10] OGASAWARA, T., OHNO, M. KARAKI, K.: One-way image transmission with a pair of multimode optical fibers and a phase-conjugate mirror. *Optics Letters*, vol. 1995, no. Vol.20, 1995: pp. 2435–2437, Available from: doi:10.1364/OL.20.002435.

[11] GOVER, A., LEE, C. P. YARIV, A.: Direct transmission of pictorial information in multimode optical fibers*. *Journal of the Optical Society of America*, vol. 1976, no. Vol.66, 1976: pp. 306–311, Available from: doi:10.1364/JOSA.66.000306.

[12] EGGLETON, B. J. et al.: Multimode fibres. In *SPIE Micro+Nano Materials, Devices, and Applications*, vol. 2015, Sydney,New South Wales, Australia: Sydney, 2015, pp. 1–6, Available from: doi:10.1117/12.2202355.

[13] LEITE, I. T. et al.: Three-dimensional holographic optical manipulation through a high-numerical-aperture soft-glass multimode fibre. *Nature Photonics*, vol. 2018, no. 12, 2018: pp. 33–39, Available from: doi:10.1038/s41566-017-0053-8.

[14] A schematic diagram of the SLM LCoS panel. *Thorlabs, Inc.* 1999. URL <https://www.thorlabs.com/images/tabimages/SLM_Diagram_A1-780.gif>

[15] WANG, D. et al.: Focusing through dynamic tissue with millisecond digital optical phase conjugation. *Optica*, vol. 2015, no. 8, 2015: pp. 728–735, Available from: doi:10.1364/OPTICA.2.000728.

[16] LEE, W. H.: Sampled Fourier Transform Hologram Generated by Computer. *Applied Optics*, vol. 1970, no. Vol. 9, 1970: pp. 639–643, Available from: doi:10.1364/AO.9.000639.

[17] BURCKHARDT, C. B.: A Simplification of Lee's Method of Generating Holograms by Computer. *Applied Optics*, vol. 1970, no. Vol. 9, 1970: pp. 1949–1949, Available from: doi:10.1364/AO.9.001949.

[18] DAVIS, J. A. et al.: Encoding amplitude information onto phase-only filters. *Applied Optics*, vol. 1999, no. Vol. 38, 1999: pp. 5004–5013, Available from: doi:10.1364/AO.38.005004.

[19] Wavefront shaping techniques in complex media. *Wavefrontshaping.org*. 2018. URL <http://wavefrontshaping.net/index.php/63-community/tutorials/phase-measurement/94-off-axis-holography>

[20] VELLEKOOP, I. M. MOSK, A. P.: Focusing coherent light through opaque strongly scattering media. *Optics Letters*, vol. 2007, no. Vol. 32, 2007: pp. 2309–2311, Available from: doi:10.1364/OL.32.002309.

[21] BEENAKKER, C. W. J.: Random-matrix theory of quantum transport. *Reviews of Modern Physics*, vol. 1997, no. Vol. 69, 1997: pp. 732–798, Available from: doi:10.1103/RevModPhys.69.731.

[22] MUKOHZAKA, N. et al.: Diffraction efficiency analysis of a parallel-aligned nematic-liquid-crystal spatial light modulator. *Applied Optics*, vol. 1994, no. Vol. 33, 1994: pp. 2804–2811, Available from: doi:10.1364/AO.33.002804.

[23] YANG, D.-K. WU, S.-T.: *Fundamentals of liquid crystal devices*. Chichester, West Sussex, United Kingdom: Wiley, second edition edition, 2015, ISBN 978-111-8752-005.

[24] POON, T.-C. BANERJEE, P. P.: *Contemporary optical image processing with MATLAB*. New York: Elsevier Science Ltd., first edition, 2001, ISBN 978-008-0437-880.

[25] Modulation Transfer Function. *Nikon Instruments Inc.* 2018. URL <https://www.microscopyu.com/microscopy-basics/modulation-transfer-function>

[26] GOLDSMITH, P. F.: Quasioptical Systems: Gaussian Beam Quasioptical Propogation and Applications. In *Quasioptical systems*, Piscataway, NJ: IEEE Press, second edition, c1998, ISBN 978-0-7803-3439-7, pp. 9–38.

[27] PASCHOTTA, D. R.: Gaussian Beams. *RP Photonics Consulting GmbH*. 2015. URL <https://www.rp-photonics.com/gaussian_beams.html>

[28] DRÈGE, E. M., SKINNER, N. G. BYRNE, D. M.: Analytical far-field divergence angle of a truncated Gaussian beam. *Applied Optics*, vol. 2000, no. Vol. 39, 2000: pp. 4918–4925, Available from: doi:10.1364/AO.39.004918.

[29] LI, Y.: Degeneracy in the Fraunhofer diffraction of truncated Gaussian beams. *Journal of the Optical Society of America A*, vol. 1987, no. Vol. 4, 1987: pp. 1237–1242, Available from: doi:10.1364/JOSAA.4.001237.

[30] SCHMIDT, J. D.: *Numerical simulation of optical wave propagation with examples in MATLAB*. Bellingham, Wash.: SPIE, first edition, c2010, ISBN 978-081-9483-263.

[31] PELI, E.: Contrast in complex images. *Journal of the Optical Society of America A*, vol. 1990, no. Vol. 7, 1990: pp. 2032–2040, Available from: doi:10.1364/JOSAA.7.002032.

Abbreviations

CCD ..... Charge-Coupled Device

DM ..... Diffraction Mask

DMD ..... Deformable Micro-Mirror Device

FFT ..... 2D Fast Fourier Transform

FWHM ..... Full-Width-Half-Maximum

HWP ..... Half Wave Plate

LC-SLM ..... Liquid-Crystal Spatial Light Modulator

LP ..... Linearly Polarized Modes

MEMS ..... Micro Electro-Mechanical Systems

MMF ..... Multimode Fiber

MTF ..... Modulation Transfer Function

NA ..... Numerical Aperture

OF ..... Overfilling Factor

PIM ..... Propagation Invariant Mode

QWP ..... Quarter Wave Plate

SF ..... Spatial Frequency

SLM ..... Spatial Light Modulator

T ..... Transmission Matrix

TIR ..... Total Internal Reflection

VI ..... Virtual Instrument

VS ..... Virtual Set-Up